CHARLES UNIVERSITY

Faculty of Science

Study programme: Inorganic Chemistry

Mgr. Jan Hynek

Porphyrin-based porous frameworks
Porfyrinové porézní struktury

Ph.D. Thesis

Supervisor: Ing. Kamil Lang, CSc.

Consultants: RNDr. Jan Demel, Ph.D.

Doc. RNDr. Jiří Mosinger, Ph.D.

Prague, 2018

Prohlášení:

Prohlašuji, že jsem závěrečnou práci zpracoval samostatně a že jsem uvedl všechny použité informační zdroje a literaturu. Tato práce ani její podstatná část nebyla předložena k získání jiného nebo stejného akademického titulu.

Declaration:

Hereby I declare that this Thesis is my original work and that I have properly cited all the information resources. This work has not been submitted either for any other or for the same academic degree.

Prague, 9.12.2018 Jan Hynek

Acknowledgement

I am deeply grateful to my supervisors Ing. Kamil Lang, CSc. and RNDr. Jan Demel, Ph.D. for their help during my doctoral research.

I am also grateful to Ing. Jaroslav Zelenka, Ph.D. and Ing. Martina Koncošová for doing the biological experiments, Ing. Jiří Rathouský, CSc. for measuring adsorption isotherms, and RNDr. Pavel Kubát, CSc. for measuring triplet states, singlet oxygen lifetimes and binding isotherms of porphyrins with serum albumin.

I also thank the Czech Science Foundation (GAČR) and the Charles University Grant Agency (GAUK) for their generous financial support.

Abstract

Porous frameworks are a class of materials including metal-organic frameworks (MOFs), covalent organic frameworks (COFs) or conjugated microporous polymers (CMPs). Porous frameworks are widely studied as materials for gas storage and separation, catalysis, sensing, drug delivery, water purification, microelectronics, etc. The results presented in the Thesis document that porous frameworks with photoactive porphyrin molecules incorporated in the structure are photosensitizers of singlet oxygen, $O_2(^1\Delta_g)$, and can be used for photodynamic applications including the construction of antibacterial coatings and of organized structures for photodynamic therapy.

The Thesis presents a complex study of photophysical properties of porphyrin-based CMPs and COFs and, for the first time, demonstrates the application of porphyrin-based COFs for photodynamic inactivation of microorganisms. The CMPs and COFs were prepared by Suzuki-Miyaura cross-coupling and Schiff base formation, respectively. The materials were characterized by IR and solid-state NMR spectroscopy. The porosity of the materials was determined via N_2 adsorption. The CMPs are microporous with pore sizes varying from 1.4 to 2.1 nm and with specific surface areas up to 624 $m^2\ g^{-1}$. On the other hand, the porphyrin-based COFs are only slightly mesoporous with a specific surface area of tens $m^2\ g^{-1}$. The pores with 7 – 9 nm in diameter have a broad distribution and are attributed to structural defects rather than to organized structural voids. Both types of porous frameworks show good chemical stability and efficient production of $O_2(^1\Delta_g)$. In general, the materials with the 3D topology have higher $O_2(^1\Delta_g)$ production efficacy than those with the 2D topology, and a longer porphyrin-porphyrin distance in the structure leads to higher $O_2(^1\Delta_g)$ yields. The yields of $O_2(^1\Delta_g)$ achieved with CMPs and COFs are 3 – 5 times higher than those of porphyrin-based MOFs (MOF-525, PCN-222 and Al-TPPC MOF), mainly due to the presence of –OH groups in MOFs, which effectively quench the produced $O_2(^1\Delta_g)$. The presence of polar $–NH_2$ groups on the surface of the prepared COFs improves bacteria adhesion and enables the preparation of antibacterial coatings. The coatings effectively inhibit the growth of *Pseudomonas aeruginosa* and *Enterococcus faecalis* biofilms when irradiated with blue (460 nm) or green (525 nm) light. Hence, the porphyrinic COFs are suitable candidates for the design of antibacterial coatings.

Phosphinic acids are promising building blocks for the construction of stable MOFs. The second part of the Thesis is devoted to the synthesis of novel tetraphenylporphyrin derivatives

with phosphinic functional groups with perspective applications as linker molecules in MOFs. The introduction of phosphinic functional groups enables tuning of the properties of the molecule by varying the substituent on phosphorus atoms. Three novel porphyrin phosphinic acids substituted with methyl, phenyl, or isopropyl groups were synthesized. The analyses of triplet state lifetimes, quantum yields of $O_2(^1\Delta_g)$ formation, and lifetimes of $O_2(^1\Delta_g)$ indicate that the peripheral substitution does not affect these characteristics. In contrast, the substitution does influence other properties, such as tendency towards aggregation, hydrophobicity, and affinity to serum albumin. Thus, the isopropyl substituents are the most suitable for aggregation suppression, whereas the porphyrin with phenyl substituents is the most hydrophobic and has the highest affinity to serum albumin. These characteristics have a strong effect on the behaviour of the porphyrins in biological systems. The cellular uptake, which was studied on cancerous HeLa cells, is the highest in the case of isopropyl-substituted porphyrin. This compound has also better retention in the cells than carboxylated or sulfonated porphyrins. The prepared porphyrins are phototoxic and the tests on HeLa cells showed significant differences. The isopropyl-substituted phosphinic porphyrin shows the highest photodynamic efficacy, whereas the methyl-substituted analogue is inactive at all. The efficacy of the isopropyl-substituted phosphinic porphyrin is also higher than that of carboxylated or sulfonated derivatives. The Thesis demonstrates that the porphyrin with isopropylphosphinic groups shows the highest cellular uptake, retention in cells, and the overall photodynamic efficacy. Although the attempts to prepare MOFs based on porphyrin phosphinic acids were not successful, it was possible to bind them onto MOF nanoparticles. The resulting nanocomposites retained the photodynamic activity. It was demonstrated that these porphyrins are attractive candidates for photodynamic applications since their photodynamic efficacy can be easily tuned by the substituent on phosphorus atoms.

Abstrakt

Porézní materiály tvoří rozsáhlou skupinu zahrnující metaloorganické sítě (MOFy), kovalentní organické sítě (COFy) nebo konjugované mikroporézní polymery (CMP). Porézní struktury jsou studovány zejména jako materiály pro uskladnění a separaci plynů, katalyzátory, senzory, materiály pro distribuci léčiv, čištění vody, mikroelektroniku atd. Výsledky prezentované v disertační práci dokládají, že porézní struktury se zabudovanými fotoaktivními molekulami porfyrinů ve struktuře jsou fotosenzitizátory singletového kyslíku, $O_2(^1\Delta_g)$, a mohou být využity pro fotodynamické aplikace, např. pro přípravu antimikrobiálních povrchů nebo organizovaných struktur pro fotodynamickou terapii.

Disertační práce představuje komplexní studii fotofyzikálních vlastností porfyrinových CMP a COFů a poprvé ukazuje možnost využití porfyrinových COFů pro fotodynamickou inaktivaci mikroorganismů. Porfyrinové CMP byly připraveny pomocí Suzukiho-Miyaurovy spojovací reakce a porfyrinové COFy byly připraveny pomocí Schiffovy kondenzace. Materiály byly charakterizovány infračervenou spektroskopií a NMR spektroskopií v pevné fázi. Porozita materiálů byla studována měřením adsorpce N_2. Porfyrinové CMP jsou mikroporézní s velikostmi pórů od 1.4 do 2.1 nm a specifickými povrchy dosahujícími až 624 $m^2\ g^{-1}$. Naproti tomu porfyrinové COFy jsou pouze částečně mezoporézní se specifickými povrchy v řádu desítek $m^2\ g^{-1}$. Póry o průměru 7 – 9 nm v nich mají širokou distribuci a jejich původ je ve strukturních defektech spíše než v přítomnosti organizovaných dutin ve struktuře. Oba typy porézních struktur vykazují vysokou chemickou stabilitu a produkují $O_2(^1\Delta_g)$. Materiály s 3D topologií obecně produkují $O_2(^1\Delta_g)$ s vyšší účinností než materiály s 2D topologií. Větší vzdálenost mezi porfyrinovými jednotkami vede k vyšší produkci $O_2(^1\Delta_g)$. Produkce $O_2(^1\Delta_g)$ je v případě CMP a COFů 3 – 5x vyšší, než bylo prokázáno v případě porfyrinových MOFů (MOF-525, PCN-222 nebo Al-TPPC MOF), což je ovlivněno především přítomností –OH skupin v MOFech, které účinně zháší vznikající $O_2(^1\Delta_g)$. Na druhé straně přítomnost polárních $–NH_2$ skupin na povrchu COFů zlepšuje přilnavost bakterií a umožňuje přípravu antibakteriálních povrchů. Tyto povrchy při ozáření modrým (460 nm) či zeleným (525 nm) světlem účinně potlačují růst biofilmů bakterií *Pseudomonas aeruginosa* a *Enterococcus faecalis*. Porfyrinové COFy jsou tudíž vhodnými materiály pro přípravu antibakteriálních povrchů.

Fosfinové kyseliny jsou vhodnými stavebními jednotkami pro přípravu stabilních MOFů. Druhá část disertační práce je proto věnována syntéze nových derivátů tetrafenylporfyrinu

s těmito funkčními skupinami s výhledem jejich využití pro přípravu MOFů. Zavedení funkčních skupin –PR(O)OH umožňuje ladění vlastností molekul pomocí změny substituentů na atomech fosforu. Byly syntetizovány tři porfyrinové fosfinové kyseliny substituované methylovou, fenylovou a isopropylovou skupinou. Analýzou dob života tripletových stavů, kvantových výtěžků $O_2(^1\Delta_g)$ a dob života $O_2(^1\Delta_g)$ bylo zjištěno, že provedená substituce na tyto charakteristiky nemá vliv. Na druhou stranu jiné vlastnosti jsou substitucí ovlivněny, např. tendence k agregaci, hydrofobicita nebo afinita k sérovému albuminu. Isopropylové substituenty jsou nejvhodnější k potlačení agregace, zatímco porfyrin s fenylovými substituenty je nejvíce hydrofobní a vykazuje nejvyšší afinitu k sérovému albuminu. Tyto charakteristiky silně ovlivňují chování porfyrinů v biologických systémech. Buněčný příjem měřený na nádorových HeLa buňkách je nejvyšší v případě porfyrinu s isopropylovými substituenty. Tento derivát je též buňkami zachytáván více než karboxylovaný nebo sulfonovaný porfyrin. Testy fototoxicity připravených porfyrinů na HeLa buňkách ukázaly zásadní rozdíly. Porfyrinová fosfinová kyselina s isopropylovými substituenty má nejvyšší fotodynamickou účinnost, zatímco její methylový analog je zcela neaktivní. Porfyrin s isopropylovými substituenty má navíc vyšší fototoxicitu než karboxylovaný nebo sulfonovaný derivát. Disertační práce ukazuje, že porfyrinová fosfinová kyselina s isopropylovými skupinami se nejvýrazněji akumuluje v buňkách, má největší retenci, a proto vykazuje nejvyšší fotodynamickou účinnost. Ačkoliv snahy o přípravu MOFů založených na porfyrinových fosfinových kyselinách nebyly úspěšné, byla prokázána možnost jejich navázání na nanočástice MOFů. Ve výsledných nanokompozitech je zachována fotodynamická aktivita porfyrinů. Bylo prokázáno, že porfyrinové fosfinové kyseliny a jejich nanokompozity jsou vhodné pro využití ve fotodynamické terapii, neboť jejich fotodynamická účinnost může být jednoduše laděna substitucí na atomech fosforu.

List of abbreviations

DSSC	Dye-sensitized solar cells
ROS	Reactive oxygen species
UV-vis	Ultraviolet and visible spectroscopy
NIR	Near infrared
TPPC	5,10,15,20-Tetrakis(4-carboxyphenyl)porphyrin
TPPS	5,10,15,20-Tetrakis(4-sulfonatophenyl)porphyrin
MOF	Metal-organic framework
PDT	Photodynamic therapy
aPDI	Antimicrobial photodynamic inactivation
IUPAC	International Union of Pure and Applied Chemistry
SBU	Secondary building unit
BDC	Benzene-1,4-dicarboxylate
IRMOF	Isoreticular metal-organic framework
MIL	Materials of Institut Lavoisier
UiO	Universitetet i Oslo
ICR	Inorganic chemistry Rez
PBPA	Phenylene-1,4-bis(methylphosphinic acid)
PCN	Porous coordination network
COF	Covalent organic framework
Pc	Phthalocyanine
PBBA	Phenylene-1,4-bis(boronic acid)
CON	Covalent organic nanosheet
CMP	Conjugated microporous polymer
POP	Porous organic polymer
PAF	Porous aromatic framework
PIM	Polymer of intrinsic microporosity
MRI	Magnetic resonance imaging
TPP	5,10,15,20-Tetraphenylporphyrin
DPP	10,20-Diphenylporphyrin
DDQ	2,3-dichloro-5,6-dicyano-1,4-benzoquinone
IR	Infrared
MAS	Magic angle spinning
NMR	Nuclear magnetic resonance
XRD	X-ray diffraction
BET	Brunauer-Emmet-Teller
NLDFT	Non-local density functional theory
TPPBr	5,10,15,20-Tetrakis(4-bromophenyl)porphyrin
HRMS	High-resolution mass spectrometry

HSA	Human serum albumin
MRC	Medical Research Council
EC_{50}	Half maximal effective concentration

Table of contents

1 Introduction

1.1 Porphyrins

Porphyrins are macrocyclic organic compounds composed of four pyrrole rings connected via four 4 bridging carbon atoms. The simplest example of porphyrins is porphine, which is just the bare skeleton without any further substituents. This molecule can be substituted either on 8 pyrrole positions (β-positions) or on bridging carbons (*meso*-positions), see Figure 1.

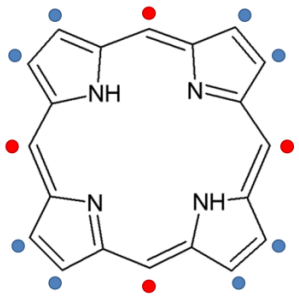

Figure 1. Structural formula of porphine with marked β-positions(●) and *meso*-positions(●).

Substitution with bulky groups is a useful tool to diminish π-π stacking of the molecules and increase their solubility and introduction of polar groups can change the character of the molecule from hydrophobic to more hydrophilic. Due to the presence of 4 nitrogen atoms, porphyrins can form coordination compounds with a wide range of metals. The coordination process is accompanied by the loss of 2 protons from the original free Lewis base. These coordination compounds play an important role in many biological systems. The most important is the coordination compound with iron called haem. Haem is a component of haemoglobin, a red pigment in blood with the function of O_2 and CO_2 transport, but also other haemoproteins (myoglobin, cytochromes, catalases, haem peroxidase and endothelial nitric oxidase synthase). Magnesium complex of porphyrin is an important part of chlorophylls, green-coloured light absorbers in the CO_2 fixation process in plants. Apart from porphyrins, several derived macrocyclic compounds also occur in biological systems. Applications of synthetic porphyrins take advantage of their properties: redox properties of porphyrin complexes with Mn, Fe, or Co are utilized in catalysis of oxidation reactions, large conjugated electron system enables a potential use for molecular electronics and photonics, strong absorption of visible light is good for harvesting solar radiation to be further transferred to electricity in dye-sensitized solar cells (DSSC),[1] and high probability of intersystem crossing enables transfer of light energy to surrounding oxygen molecules, leading to the formation of reactive oxygen species (ROS), which opens door to a wide variety of other applications.

1.2 Singlet oxygen

Oxygen molecule in the ground electronic state ($^3\Sigma_g^-$) has two unpaired electrons localized in the highest occupied molecular orbitals $\pi_{x,z}^*$. The rearrangement of spin of one of the electrons can lead to two possible states (see Figure 2). In the case of the $^1\Sigma_g^+$ state each of the paired electrons is localized in a different orbital, and the energy difference between the ground state and $^1\Sigma_g^+$ is 157 kJ mol^{-1}. The second possibility is the formation of the $^1\Delta_g$ state where a pair of electrons is in the same orbital. The $^1\Delta_g$ state is 94 kJ mol^{-1} above the ground state. Due to a very short lifetime of $^1\Sigma_g^+$, its chemical importance is negligible. For this reason, when analysing singlet oxygen reactivity, it is meant the $^1\Delta_g$ state. The consequence of the higher energy of $O_2(^1\Delta_g)$ in comparison with the ground state is enhanced reactivity. Singlet oxygen belongs with peroxides, superoxide and hydroxyl radical to the group of ROS.[2]

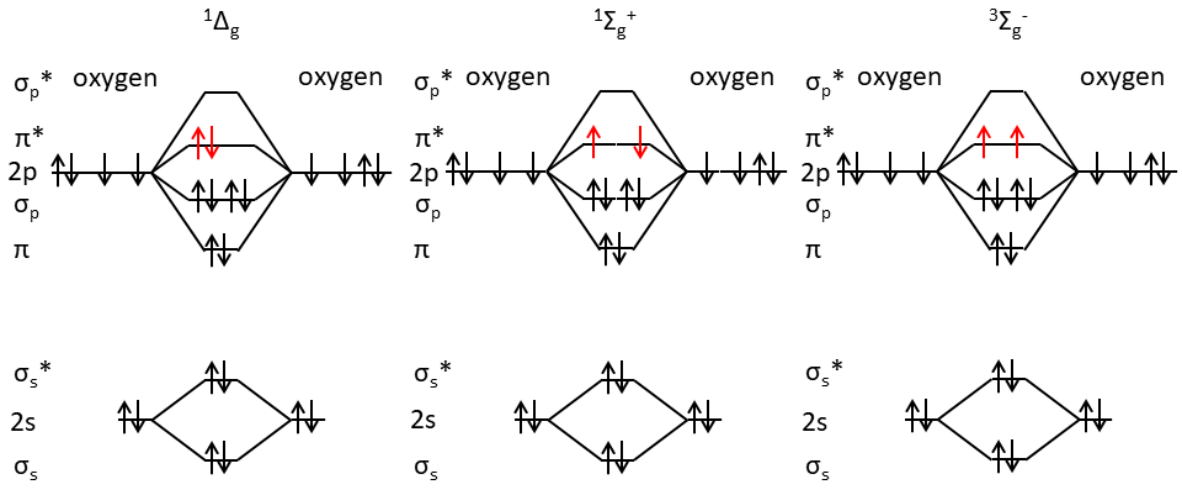

Figure 2. Electronic states of molecular oxygen.

Singlet oxygen can be formed by several chemical, physical, and biological processes. Chemical methods involve decomposition of *in situ* prepared peroxocompounds (1) or ozonides (2), reaction of hypochlorite with hydrogen peroxide (3), or thermolysis of an endoperoxide (4).

(1) $Na_2MoO_4 + 4\,H_2O_2 \rightarrow Na_2[Mo(O_2)_4] + 4\,H_2O \rightarrow Na_2MoO_4 + 4\,H_2O + 2\,O_2(\,^1\Delta_g)$

(2) $(RO)_3P + O_3 \rightarrow (RO)_3PO_3 \rightarrow (RO)_3PO + O_2(\,^1\Delta_g)$

(3) $H_2O_2 + NaClO \rightarrow O_2\left(\,^1\Delta_g\right) + NaCl + H_2O$

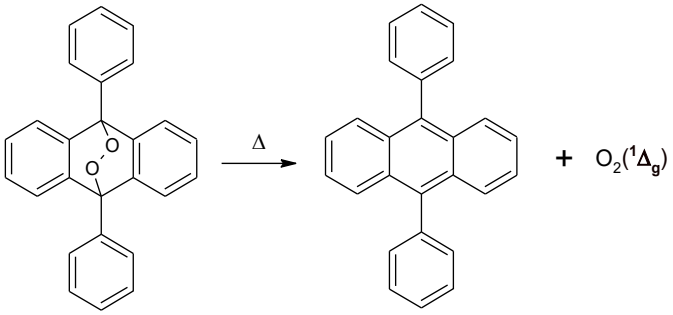

(4)

Reaction (3) is also biologically important because it proceeds during phagocytosis where ClO^- formed by myeloperoxidase reacts with hydrogen peroxide in tissues.[3]

A very effective method of the $O_2(^1\Delta_g)$ generation is photosensitization (Figure 3). This process involves a dye molecule which is excited by absorption of UV-vis or NIR radiation into a higher electronic state. After excitation, the molecule can either undergo radiative relaxation (fluorescence, 5), non-radiative relaxation (internal conversion), or form a triplet excited state via intersystem crossing (6). Triplet states play a crucial role in photosensitization because they can readily react with oxygen molecules leading to $O_2(^1\Delta_g)$ (7). This is due to the fact that the reaction of a photosenzitizer in the singlet excited state with $O_2(^3\Sigma_g^-)$ is not spin allowed, whereas the reaction of a photosenzitizer in the triplet excited state is spin allowed. In parallel, the triplet excited state can undergo a spin forbidden radiative relaxation (phosphorescence, 8). Produced $O_2(^1\Delta_g)$ undergoes radiative relaxation connected with phosphorescence at 1270 nm (9), which is utilized for direct detection of $O_2(^1\Delta_g)$, including measurement of its lifetime.

(5) $^1\text{Sens}^* \rightarrow {}^1\text{Sens} + h\nu_F$

(6) $^1\text{Sens}^* \rightarrow {}^3\text{Sens}$

(7) $^3\text{Sens}^* + O_2(\,^3\Sigma_g^-) \rightarrow {}^1\text{Sens} + O_2(\,^1\Delta_g)$

(8) $^3\text{Sens}^* \rightarrow {}^1\text{Sens} + h\nu_P$

(9) $O_2(\,^1\Delta_g) \rightarrow O_2(\,^3\Sigma_g^-) + h\nu_P$

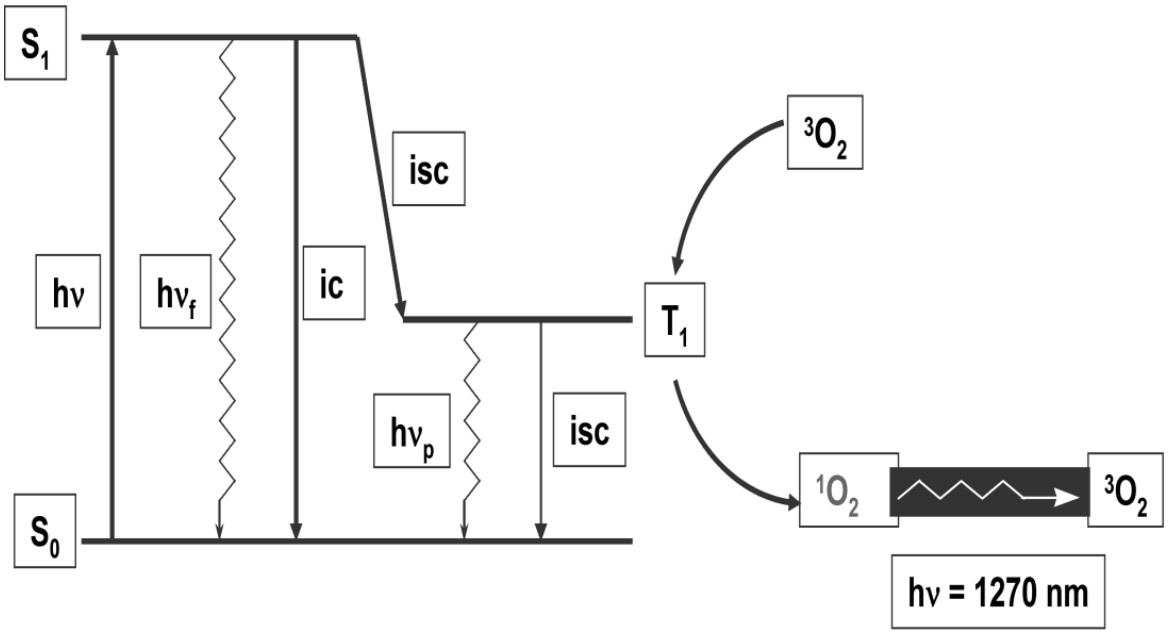

Figure 3. Mechanism of photosensitized production of $O_2(^1\Delta_g)$: $h\nu$ stands for light absorption, $h\nu_F$ is fluorescence, *ic* is internal conversion, *isc* stands for intersystem crossing, and $h\nu_P$ is phosphorescence.[4]

Photosensitized reactions with oxygen can be divided into 2 groups: type I and II.[5] Type I reactions involve quenching of excited states by substrate or solvent molecules, which form radicals and react with molecular oxygen afterwards (10). In contrast, type II reactions proceed via $O_2(^1\Delta_g)$ or superoxide anion radical formation (7, 11), followed by oxidation of the substrate by these oxidation agents.[6]

(10) $\mathrm{Sens}^* + \mathrm{Q} \rightarrow \mathrm{Sens}^+ + \mathrm{Q}\cdot^-$

(11) $\mathrm{Sens}^* + \mathrm{O_2}\left(\,^3\Sigma_g^-\right) \rightarrow \mathrm{Sens}^+ + \mathrm{O_2}\cdot^-$

Porphyrins and their coordination compounds with some metals (e.g., Pd, Zn) are powerful photosensitizers of $O_2(^1\Delta_g)$. The drawback of porphyrins is the fact that they tend to form closely stacked assemblies held together by strong π-π interactions. For this reason, they have neither luminescence nor $O_2(^1\Delta_g)$ production in the solid state. This propensity makes preparation of solid state porphyrin photosensitizers a challenge. One of the possible approaches is intercalation of porphyrin anions (carboxylate – TPPC or sulfonate – TPPS, see Figure 4) into layered hydroxides.[7,8] The porphyrin-layered hydroxide hybrids do produce $O_2(^1\Delta_g)$, however, its lifetime is negatively influenced by quenching by –OH groups present in the proximity of the porphyrin units.[9]

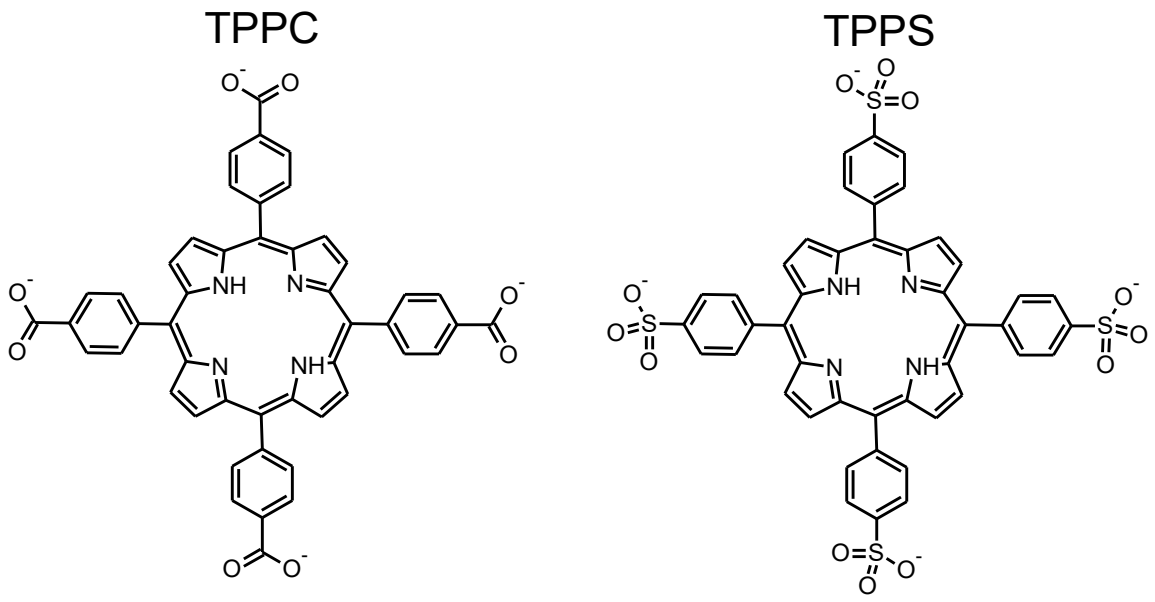

Figure 4. Molecular structures of the anions of 5,10,15,20-tetrakis(4carboxyphenyl)porphyrin (TPPC, left) and 5,10,15,20-tetrakis(4-sulfonatophenyl)porphyrin (TPPS, right).

In the case of layered europium hydroxides, a change in reaction conditions leads to the formation of a 3D non-porous material.[10] After this first example of a metal-organic framework (MOF) with proved ability to produce $O_2(^1\Delta_g)$, many MOF structures were utilized for applications where singlet oxygen plays a crucial role.

1.3 Photodynamic therapy

Singlet oxygen is a strong oxidation agent which can oxidize important biomolecules such as amino acids, fatty acids, and cholesterol. This oxidative stress can lead to a cell death.[11] For example, the production of $O_2(^1\Delta_g)$ by non-metalated porphyrin in organisms causes a disease called porphyria.[12] On the other hand, the cytotoxic effect of $O_2(^1\Delta_g)$ can be intentionally employed for killing tumour cells[13] or microorganisms.[14] The former process is called photodynamic therapy (PDT). An effective photosensitizer for PDT has to fulfil several criteria, mainly: stability and good solubility in biological media, efficient productivity of ROS when irradiated by light, the absence of dark toxicity, light absorption ideally in NIR region in order to achieve good tissue penetration, and last but not least chemical purity.[15] The first generation of photosensitizers for PDT was based on hematoporphyrin derivatives, under commercial name Photophrin®.[16] The need for overcoming disadvantages of hematoporphyrins, such as poor chemical purity, long life-time causing prolonged skin photosensitization, or activation wavelength too short for good tissue penetration, led to the

development of the second generation of photosensitizers, which included both peripheral functionalization and modification of the porphyrin core.[17] The efficiency of photosensitizers for PDT can be further improved by introduction of groups selectively targeting subcellular compartments. Bioconjugates of photosensitizers with, e.g., lipoproteins or folate molecules represent the third generation of photosensitizers for PDT.[18] Recent developments favour complex supramolecular assemblies containing second generation photosensitizers encapsulated in nanosized delivery systems.[19]

An analogous process aimed at microbial cells is called antimicrobial photodynamic inactivation (aPDI). In comparison with the standard use of antibiotics, aPDI has several advantages; it works regardless of the antibiotic resistance, it does not induce resistance in bacteria, and a photosensitizer can be applied locally. To be applicable for aPDI, a photosensitizer has to fulfil similar conditions as described for cancer PDT, such as no dark toxicity, high quantum yields of ROS, and high molar absorption coefficient at wavelengths which penetrate well through tissues. Additionally, the systems should demonstrate good selectivity towards microbial cells. Positive charge of photosensitizers can be beneficial, because it enhances their adhesion to typically negatively charged microbial cell walls. The suitable sources of the positive charge are quaternary nitrogen atoms or basic amino groups.[20]

1.4 Porous materials

Porous materials are substances containing voids. Usually, the matrix of a porous material is solid and the voids are filled with a liquid or gas. Many materials occurring in the nature can be considered to be porous materials, e.g., rocks and soils, zeolites, biological tissues (wood, cork, bones etc.). The most important characteristic of porous materials is the size and shape of the pores. According to the typical pore sizes, porous materials are divided into 3 categories: microporous (pore size < 2 nm), mesoporous (pore size 2 – 50 nm), and macroporous (pore size > 50 nm). Since natural porous materials contain voids with predefined size and shape, preparation of synthetic materials with tuneable pore properties became a topic of great interest.

1.4.1 Metal-organic frameworks

According to the IUPAC nomenclature, coordination polymers are coordination compounds extending in 1, 2 or 3 dimensions through coordination bonds. Coordination networks are coordination compounds extending in 1 dimension through coordination bonds with cross-links between two or more individual chains, loops or spiro-links, or coordination compounds

extending in 2 or 3 dimensions through coordination bonds. Metal-organic frameworks (MOFs) are a special type of coordination polymers with an open framework containing potential voids. MOFs are composed of metal cations or their clusters called secondary building units (SBUs) linked by bi- or multidentate organic ligands, and usually they are crystalline.[21]

MOFs were discovered by Yaghi *et al.* in 1995.[22] In 1999, the same group published the structure of MOF-5 with chemical composition $Zn_4O(BDC)_3$ where BDC stands for benzene-1,4-dicarboxylate linkers (see Figure 5). They managed to synthesize a material with a specific surface area over 2300 $m^2\ g^{-1}$.[23] Later, based on MOF-5, a new family of isoreticular MOFs (IRMOFs) with the same SBU altering the size of a linking molecule and having an additional functionality was synthesized. Additional functionalities successfully introduced on a BDC molecule include –Br, $–NH_2$ or a propyloxy- group, and BDC linkers can be easily replaced by naphthalene-2,6-dicarboxylate, biphenylene-4,4'-dicarboxylate, terphenylene-4,4''-dicarboxylate, or pyrene-2,7-dicarboxylate.[24] In spite of the structural richness and high surface area of IRMOFs, their practical application is limited because they all suffer from low hydrolytic stability.

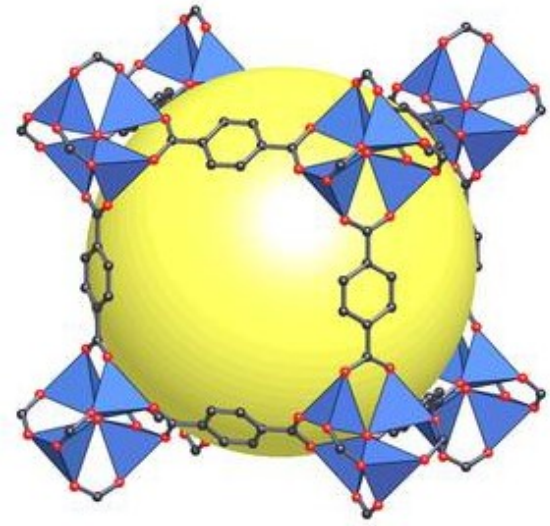

Figure 5. Structure of MOF-5 constructed from Zn_4O SBUs and benzene-1,4-dicarboxylate linkers.[24]

Another milestone in MOF chemistry was brought by Férey *et al.* who synthesized MIL-53, the first MOF based on trivalent cations with the chemical formula $Cr^{III}(OH)(BDC)$. Its flexible structure can reversibly change the porosity by more than 50 % upon hydration /dehydration. This phenomenon is called breathing effect.[25] Later, isostructural materials with

Al(III) and Fe(III) were developed. The octahedral coordination of trivalent cations instead of the tetrahedral one in the case of MOF-5 leads to the enhanced hydrolytic stability of such MOFs, however, at elevated temperature the materials often lose their porosity and turn into non-porous products.[26] The same trivalent elements and BDC linker also form the structure of MIL-101 with the chemical formula $[M_3(O)X(BDC)_3(H_2O)_2]$ (M = Cr(III), Al(III) or Fe(III), X = OH or F), which contains extra-large cavities with a diameter of 30 – 34 Å.[27]

Up to now, the most stable carboxylate MOFs are those based on Zr(IV) or other tetravalent metals (Hf(IV), Ce(IV)). The first example was UiO-66 discovered in 2008 by Cavka *et al.* [28] This material with the formula $Zr_6O_4(OH)_4(BDC)_6$ contains eight coordinated zirconium atoms with a square-antiprismatic coordination sphere. The high coordination number, high metal oxidation state together with the radius of the ions and hydrophobicity of the pores are believed to be the reasons for its exceptional stability. Another advantage of Zr-based MOFs is their structural richness. It is possible not only to replace BDC for similar ditopic ligands with larger spacers, such as biphenyl or terphenyl in UiO-67 or UiO-68 structures, respectively (see Figure 6), but also to use linkers with trigonal (e.g., benzene-1,3-tricarboxylate), tetragonal (e.g., 1,3,6,8-tetrakis(*p*-benzoate)pyrene), or even tetrahedral (4',4'',4''',4''''-methanetetrayltetrabiphenyl-4-carboxylate) topology (see Figure 7).[29]

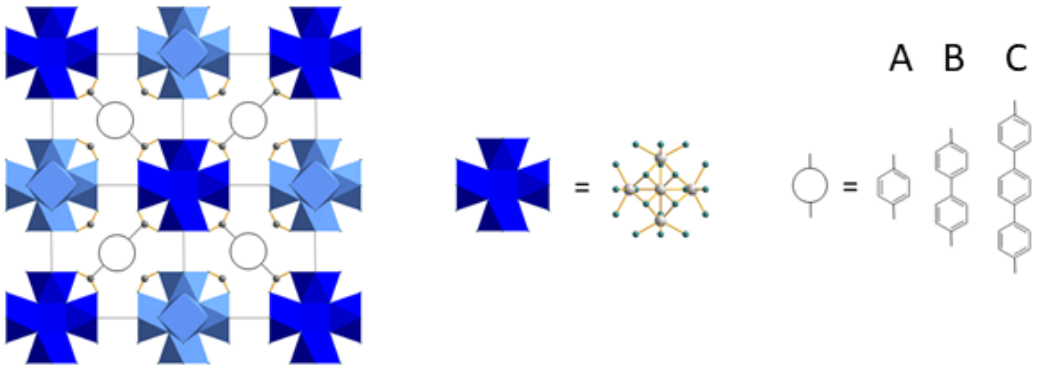

Figure 6. Schematic structure of Zr-based MOFs with increasing size of a spacer: UiO-66 (A), 67 (B) and 68 (C).

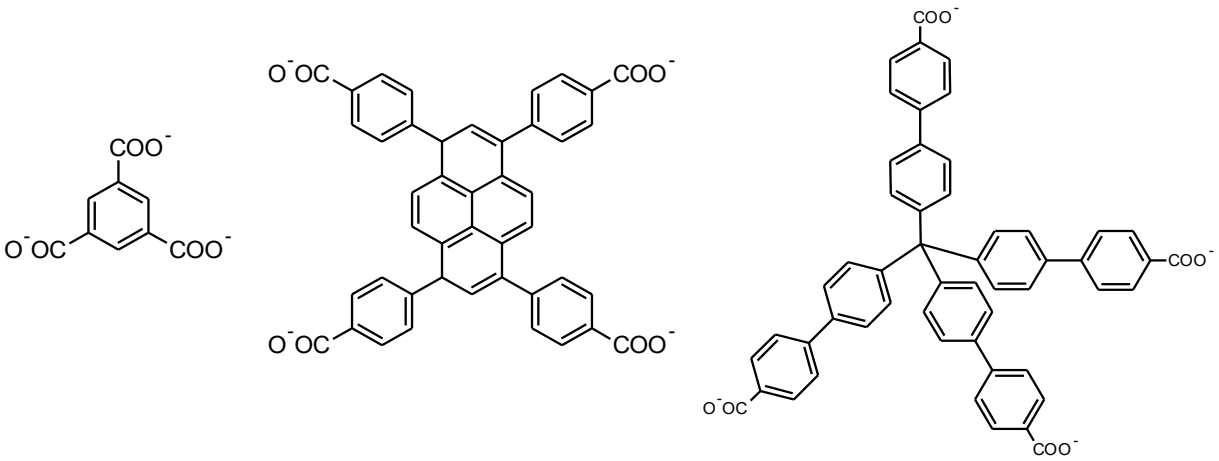

Figure 7. Examples of trigonal, tetragonal, and tetrahedral linkers utilized for the construction of Zr-based MOFs.

Recently, a new class of MOFs containing linkers bearing phosphinate groups instead of commonly used carboxylates has been developed. [30] The material ICR-2 (Inorganic Chemistry Rez) with a honeycomb hexagonal structure and the chemical formula $Fe_2(PBPA)_3$ contains chains of octahedrally coordinated Fe(III) atoms bridged by phenylene-1,4-bis(methylphosphinate) linkers (PBPA) (see Figure 8). The coordination motif of Fe(III) atoms resembles the structure of MIL-53, however, every Fe(III) ion in the structure of ICR-2 is coordinated by six oxygen atoms of the linker in contrast with only four oxygen atoms in the case of MIL-53. The remaining two coordination sites of Fe(III) in MIL-53 are occupied by bridging OH^- ligands, which are absent in the ICR-2 structure. This configuration leads to the increased hydrophobicity of the pores, which is with the strength of the phosphinate–Fe(III) coordination bond the reason for the high hydrothermal stability of ICR-2.

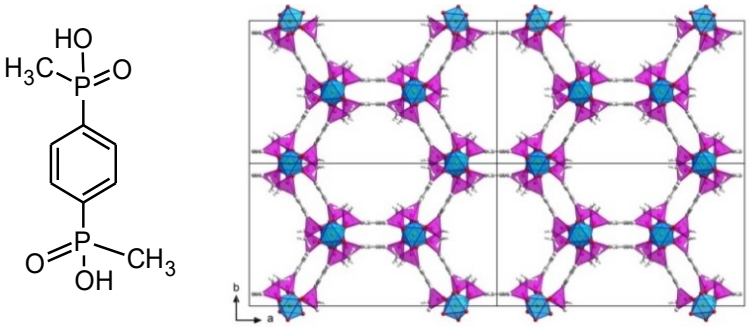

Figure 8. PBPA linker molecule (left) and the structure of the first developed phosphinate MOF ICR-2 (right).

Porphyrins substituted with donor groups are also suitable linkers for the construction of MOFs due to their rigidity, high chemical stability, and the possibility of introducing further

functional properties to the resulting material. Whereas pyridyl-substituted porphyrin tends to form 2D planar structures, carboxylate-substituted porphyrins are more likely to assemble into 3D structures. A large group of porphyrin carboxylate MOFs contain a paddle-wheel structural unit, where porphyrin molecules are assembled into planes which are interconnected by N donor molecules (e.g., bipyridine).[31] Probably, the most important porphyrin MOFs belong to the Zr-based family. Zhou *et al.* developed a series of Zr MOFs with the TPPC linker named PCN-221 up to PCN-225 differing in the topology, and hence in the SBU interconnection, which is achieved via tuning the components ratio in the reaction mixture and the amount of a modulating agent, usually a monocarboxylic acid. Independently, Yaghi *et al.* synthetized analogous series of MOFs denoted MOF-525 (see Figure 9), MOF-535 and MOF-545.[32]

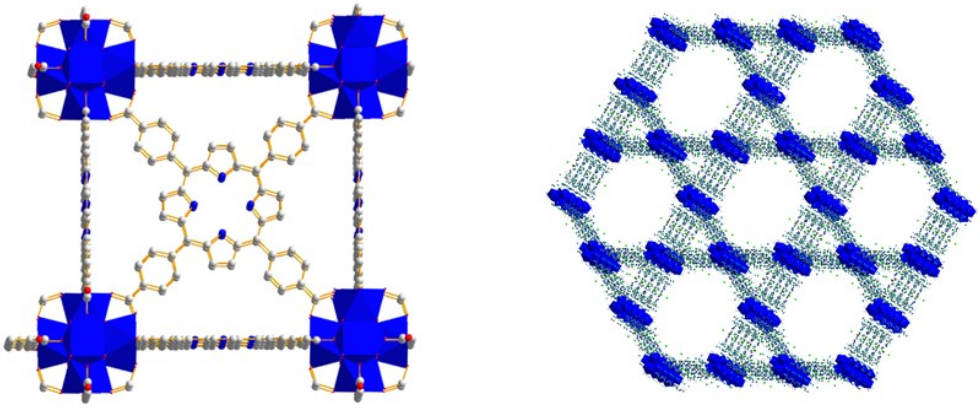

Figure 9. Structures of Zr-based porphyrin MOFs: cubic MOF-525[33] (left) and hexagonal PCN-222 (right).[34]

1.4.2 Covalent organic frameworks

Covalent organic frameworks (COFs) are organic analogues of MOFs, first introduced by Yaghi *et al.*[35] COFs contain voids, however, the building blocks are connected by covalent bonds. Apart from the different type of bonding of the building blocks, the main difference between COFs and MOFs is the fact that COFs are entirely composed of light elements (C, O, H, N, B etc.). Because of the claim for crystalline materials with high structural precision, the bonds connecting building blocks have to be formed reversibly, i.e., by a dynamic covalent bond formation. This process cannot be realised with the majority of common organic reactions, nevertheless, it is applicable in some types of condensation and addition reactions.[36] First COFs synthesized in 2005 by Yaghi *et al.* contained building blocks connected via boroxine or boronate ester linkage (COF-1 and COF-5, structures are given in Figure 10),[37]

Since then, B – O bonds together with C = N bonds have remained the most widely used types of linkage used for the construction of COFs.

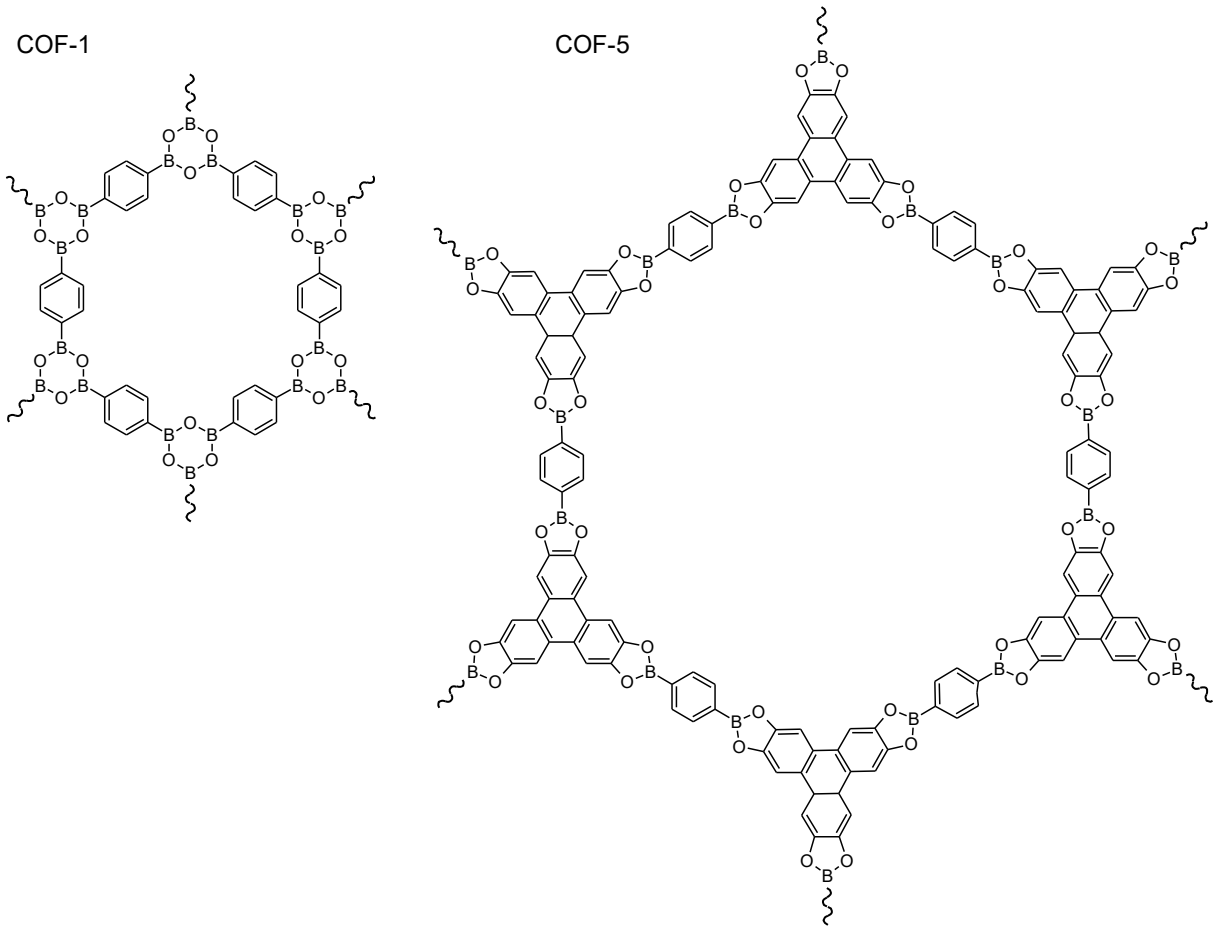

Figure 10. Structures of COFs synthesized by Yaghi *et al.*: COF-1 (left) and COF-5 (right).[37]

There are more examples of building block linkage based on the presence of boron atoms in the linking motif (see Figure 11). The boroxine motif, which is a heterocyclic six-membered ring with a regular alternation of B and O atoms, is formed via a self-condensation of three molecules of a boronic acid. A similar type of building blocks connection is a borazine linkage, which results from a self-condensation of three molecules of BH_3 adduct with an amine molecule and contains B – N bonds instead of B – O.[38] In contrast, the formation of a boronate ester requires two components – a boronic acid and a vicinal diol. Other types of building blocks connection originating from a two component reaction are borosilicate COFs connected via triangles of tetrahedra[39] and spiroborate COFs with sp^3 hybridized negatively charged boron nodes.[40]

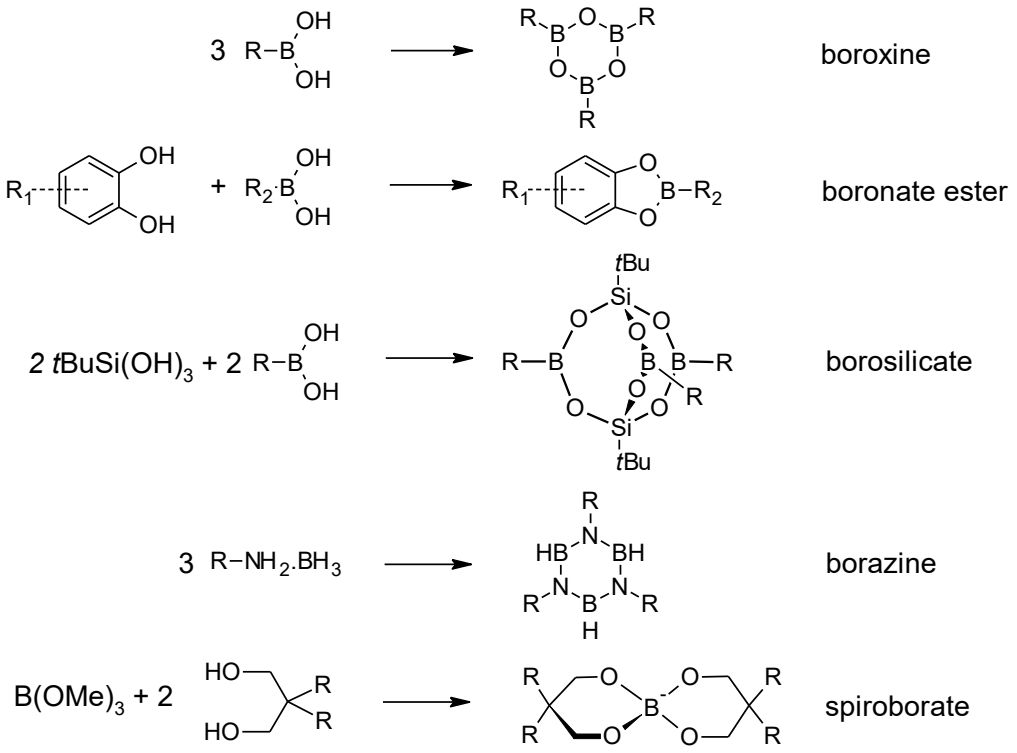

Figure 11. Types of boron-based linkages used for the construction of COFs.

Although the B – O bonding provides numerous rigid and thermally robust structures, they decompose in acidic or basic environment and in some cases even their destruction by moisture in the air was reported. In comparison with the B – O linked COFs, materials with building blocks connected via C = N bonds show enhanced stability.[41] For the formation of C = N bonds, several types of imine condensation can be used. In 2009, first COFs employing the C = N bonding were prepared using a combination of an aldehyde and an amine, which led to the formation of a classical Schiff base.[42] Instead of amines, hydrazine or hydrazides of carboxylic acids can be used providing azine[43] and hydrazone[44] COFs, respectively (see Figure 12).

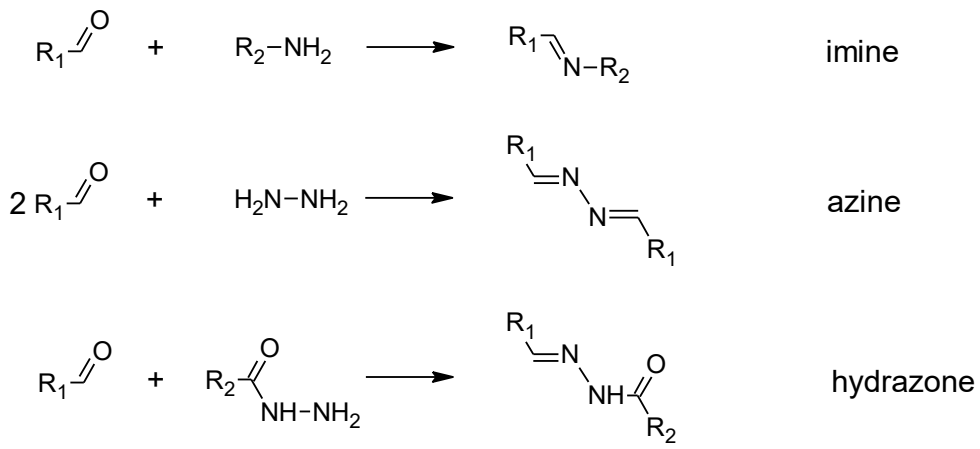

Figure 12. Types of C = N linked COFs.

COFs can have both 2D and 3D topologies. Materials called 2D COFs are composed of covalently bonded planar sheets stacked together in the third dimension by π-π interactions (see Figure 13). For the preparation of 2D COFs, trisubstituted benzenes, tetrasubstituted porphyrins, or other precursors with planar geometry and C_2, C_3, C_4 or C_6 symmetry are used (see Figure 14). The early COFs were built up from simple aromatic molecules.[37,45] In 2010, the synthesis of a boronyl ester linked 2D framework named Pc-PBBA COF was reported, which was the first example of a COF with phtalocyanine building blocks.[46] Later on, an analogous framework with porphyrin was developed.[47] Large aromatic system containing COFs were found to be photoconductive and therefore applicable in light-harvesting devices.[48] Therefore, porphyrin- and phtalocyanine-based COFs started to be intensively studied. Similarly, 2D COFs with imine connection were described (e.g. COF-366, see Figure 15)[49] and their crystallinity and chemical stability was furtherly increased by introducing –OH groups forming hydrogen bonds with the imine nitrogen atoms on the building blocks.[50,51] An interesting approach to improve charge carrier mobility was developed by Nagai *et al.*, who employed the unique amphionic squaraine type of building blocks bonding.[52] 2D COFs can be also prepared in the form of single or few layer thick covalent organic nanosheets (CONs) via either bottom-up growth on solid-vapor interfaces[53] or top-down process of delamination of the respective layers by ultrasonication of the parent COF in a suitable solvent.[54]

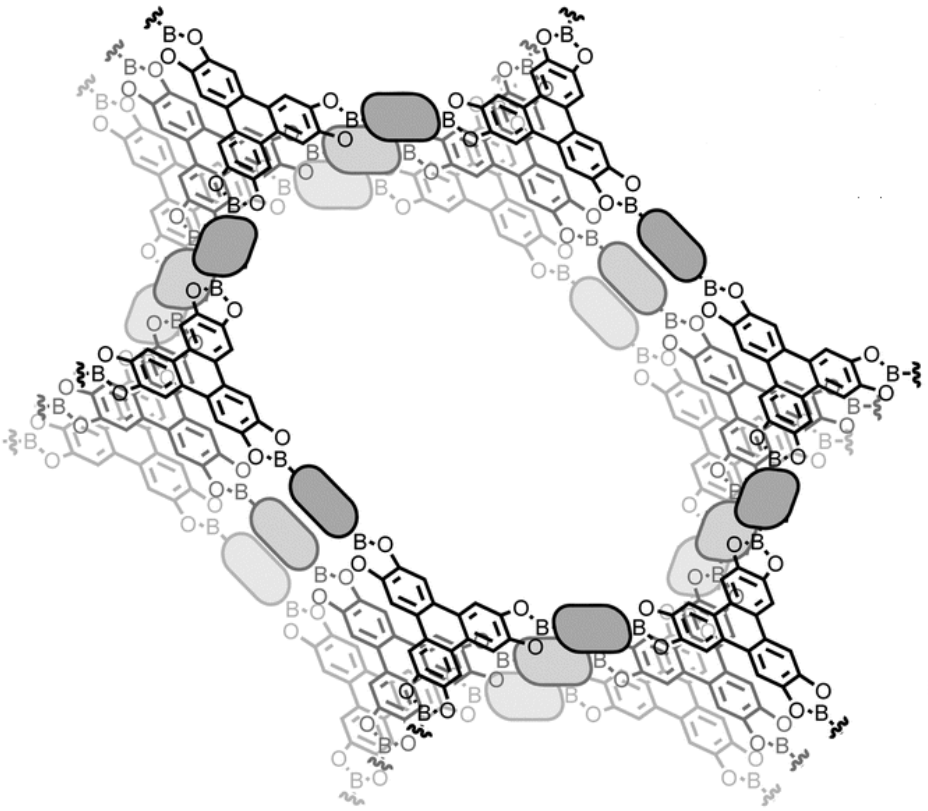

Figure 13. Structure of COF-5 showing the stacking of covalently bonded planar sheets.[55]

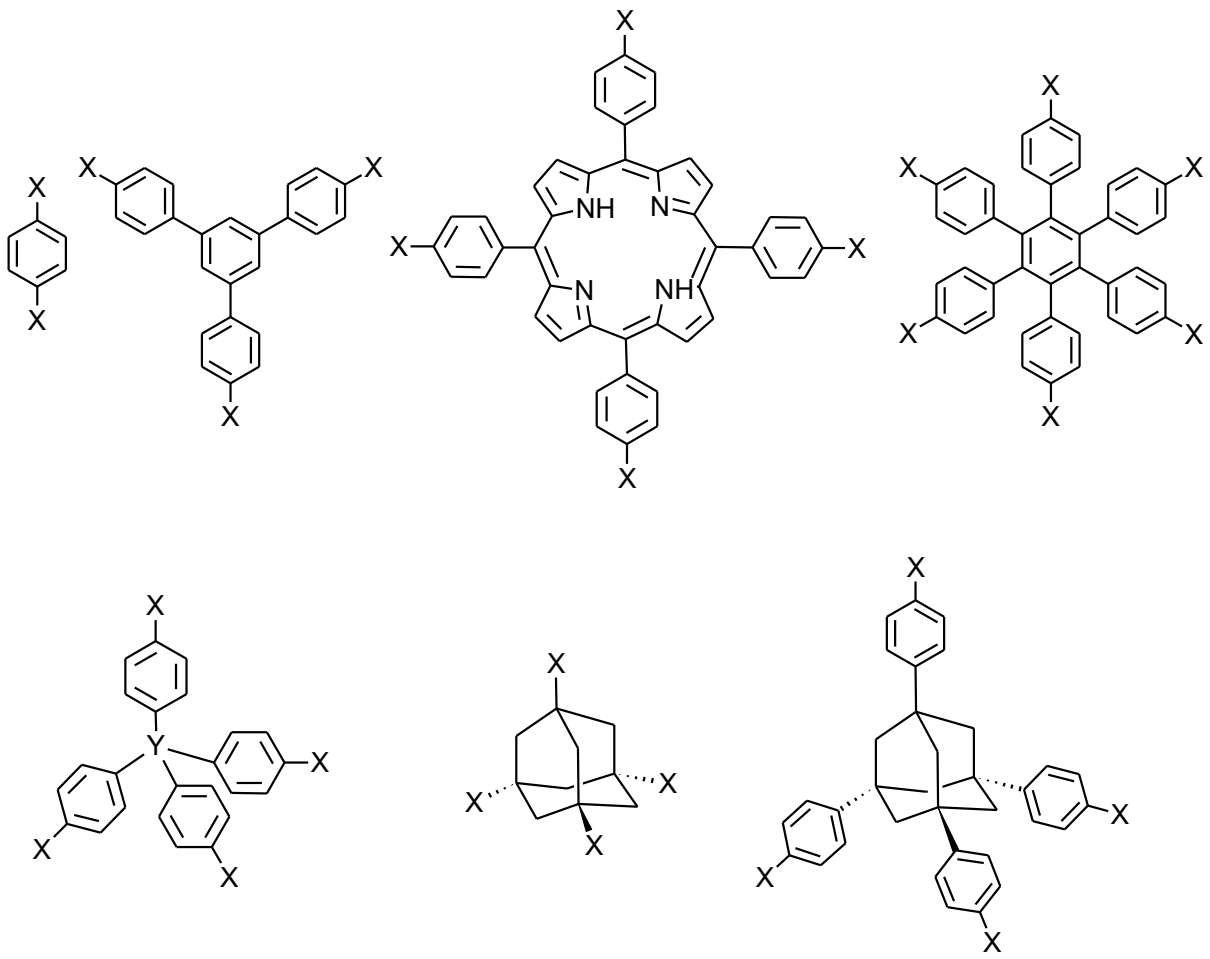

Figure 14. Examples of precursors used for the construction of 2D COFs with the C_2, C_3, C_4 and C_6 symmetry (top) and precursors for 3D COFs (bottom).

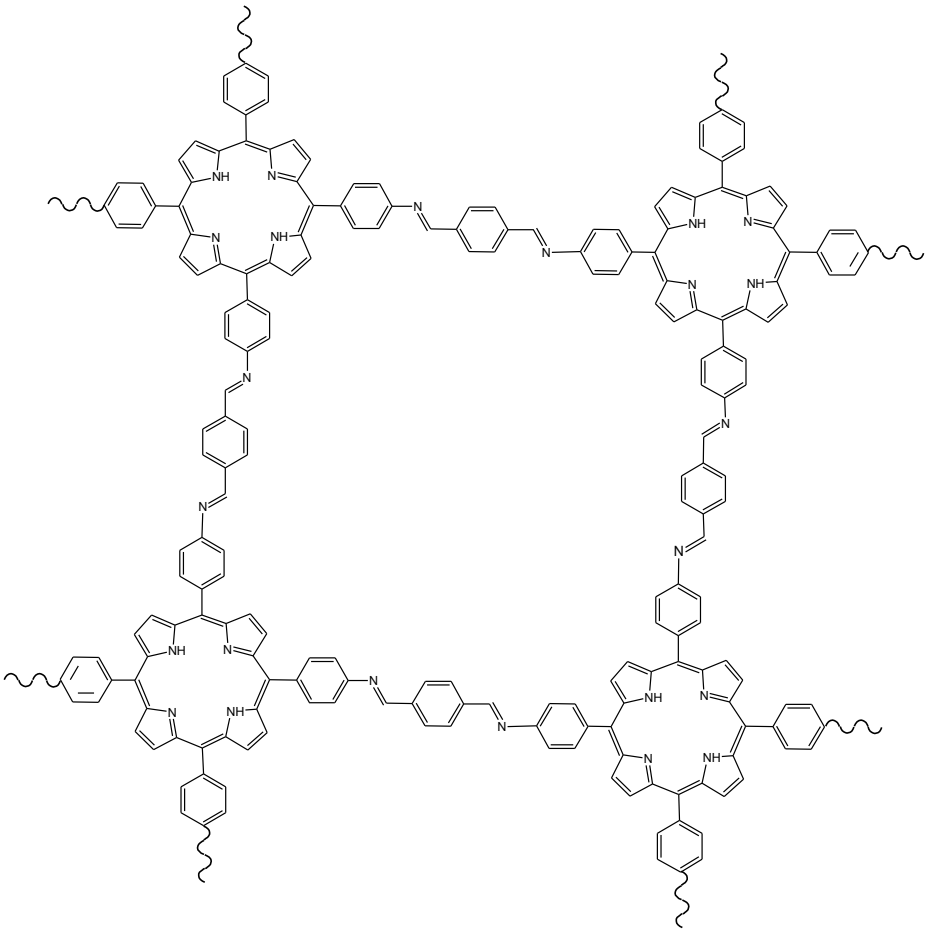

Figure 15. Structure of imine-linked 2D porphyrin-based COF-366.

Whereas numerous examples of 2D COFs have been already synthesized, the number of reported 3D COFs is still limited. In contrast with planar molecules serving for the construction of 2D frameworks, 3D COFs have to contain building blocks extended in all three directions. This can be achieved by the presence of at least one sp^3 hybridized atom carbon, resulting in the tetrahedral geometry of the building blocks. Precursors, which have been ever used for 3D COFs construction, are exclusively based on tetraphenyl methane, its silicon analogue tetraphenyl silane or adamantane (see Figure 14). The earliest 3D COFs were prepared by either self-condensation of tetrakis(4-dihydroxyboronylphenyl)methane (COF-102) and tetrakis(4-dihydroxyboronylphenyl)silane (COF-103), or by their co-condensation with trigonal 2,3,6,7,10,11-hexahydroxytriphenylene (COF-105 and COF-108).[56] The first 3D COF with imine connectivities was COF-303, which combined tetrahedral building blocks with linear ones, adopting a diamond-like structure.[42] Later, isostructural materials with the boronyl ester[57] or imide[58] building block connections were also described. Recently, a new class of 3D COFs containing tetrasubstituted pyrene[59] or porphyrin[60] has been developed.

1.4.3 Amorphous porous polymers

Another large group of porous frameworks consists of materials called conjugated microporous polymers (CMPs), porous organic polymers (POPs), porous aromatic frameworks (PAFs), or polymers of intrinsic microporosity (PIMs). Similarly to COFs, they are composed of organic building blocks, but their character is amorphous. Therefore, the number of reactions for their synthesis is not limited by the need for their dynamicity and the structure of building blocks does not necessarily have to be regular. In comparison with crystalline porous frameworks prepared by dynamic reactions (MOFs and COFs), amorphous porous polymers have enhanced chemical and thermal stability.[61] On the other hand, the consequences of their amorphous character are disordered nature and broad pore size distributions. Reactions employed for the construction of amorphous porous polymers include coupling reactions (Suzuki, Yamamoto, or Sonogashira reactions), trimerization of aromatic nitriles or alkynes, Friedel-Crafts reaction or Schiff-base formation, which can be employed for preparation of both crystalline and amorphous porous frameworks (see Figure 16). [62]

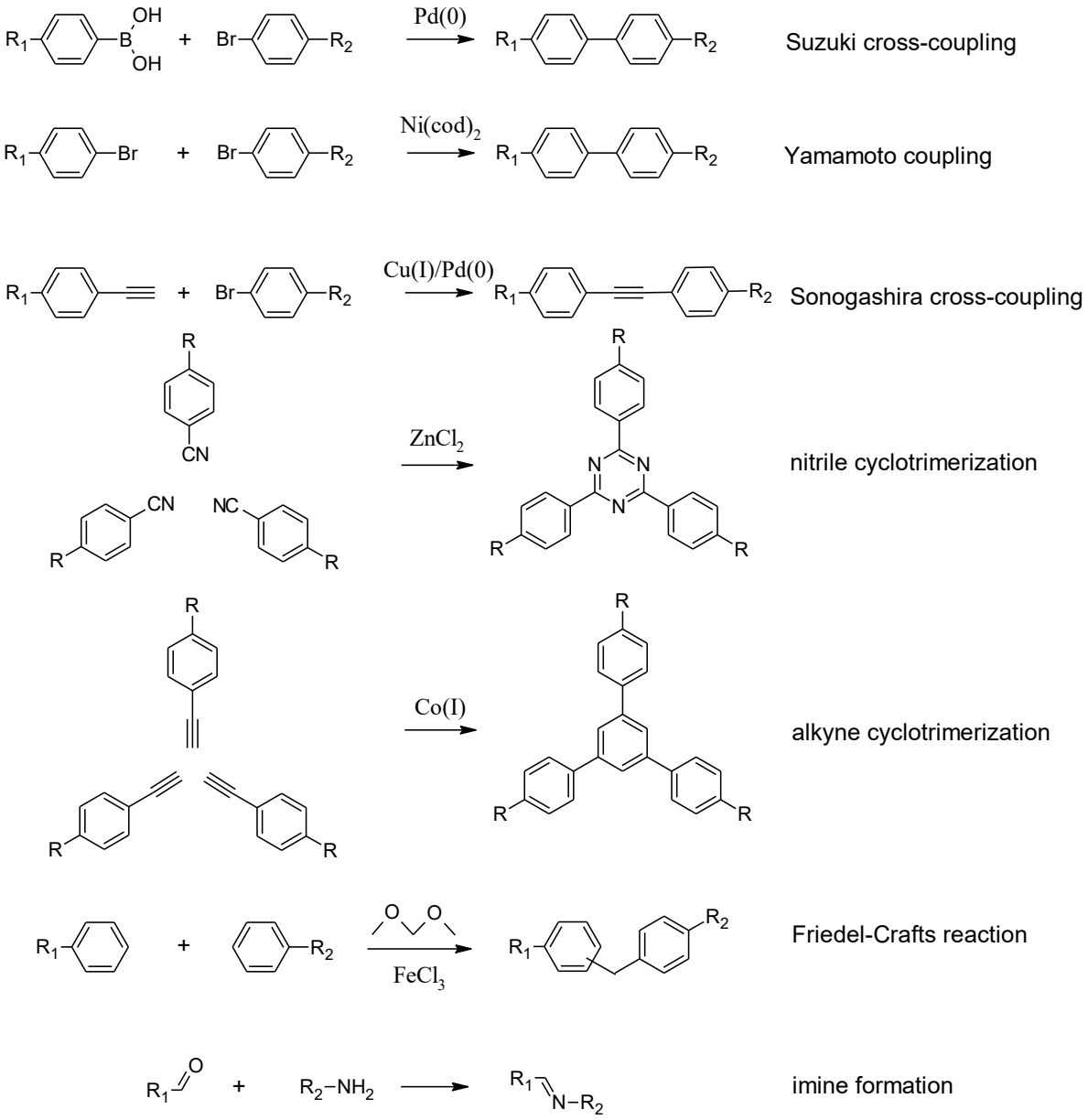

Figure 16. Examples of reactions used for the synthesis of CMPs.

Polymers with a high surface area have been known since 1990, but intensive research in the field of rigid polymer networks with microporous character began in 2002, when first porous polymers based on rigid phtalocyanine and porphyrin building blocks were described. [63,64] CMPs are a specific kind of amorphous porous polymers with a periodical arrangement of conjugated bonds between aromatic groups. First CMPs having high surface areas were synthesized by Cooper *et al.* and were composed of planar benzene rings connected via ethynylene groups.[65] Apart from planar building blocks, precursors with tetrahedral topology can be also employed, which leads to the formation of 3D diamond-like networks. An example of such material is PAF-1 prepared by [Ni(cod)$_2$] catalysed homocoupling of

tetrakis(4-bromophenyl)methane. The specific surface area of PAF-1 is comparable to the best MOFs and COFs, even despite its amorphous character.[66]

PIMs are another class of amorphous porous polymers. The porosity of these materials is caused by the presence of fused rings in the polymeric chains, which blocks free rotation along the chain backbone and preserves voids in the structure.[67]

1.4.4 Applications of porous frameworks

Originally, porous frameworks were intended to serve mainly as materials for gas storage. Because of the negative environmental effect of CO_2 and great potential of H_2 to replace fossil fuels as the dominant energy source, these two gases are the most widely studied adsorbates.[68] Moreover, different affinity of the materials towards particular gases can be utilized for their separation.[69] Another field where porous frameworks can find applications is heterogeneous catalysis. In the case of MOFs, catalytic centres can be either directly SBUs or the bridging ligands, or they can be introduced via postsynthetic modifications of MOFs.[70] In the case of non-metallic porous frameworks, these have to contain such building blocks which are catalytically active themselves.[71] Porous frameworks are also employed as supports for other heterogeneous catalysts (e.g., Pd nanoparticles catalysing coupling reactions).[72]

Apart from gas storage, gas separation, and heterogeneous catalysis, other applications of porous frameworks have been investigated. Nanoscale MOFs are studied as drug delivery systems.[73,74] Frameworks based on highly paramagnetic metals, which increase water proton relaxation rates, are studied as magnetic resonance imaging (MRI) contrast agents.[75] Porous frameworks are often employed in energy-related applications as hosts in lithium-ion batteries, supercapacitors, or platforms for solar cells,[76] especially CMPs, which contain large conjugated systems of π electrons and have semiconducting and light harvesting properties.[77]

Incorporation of porphyrin molecules into the structure of porous frameworks introduces new functionalities. Metalloporphyrin catalytic centres in the structure of either crystalline or amorphous porous frameworks can serve as catalysts in oxidation reactions.[78,79] For this purpose, porphyrins with coordinated Fe(II), Mn(III), Co(II), or Ru(III) were investigated in, e.g., epoxidation of C = C bonds, oxidation of sulphides to sulfoxides, and hydroxylation or carbonylation of C – H bonds (see Figure 17).[80]

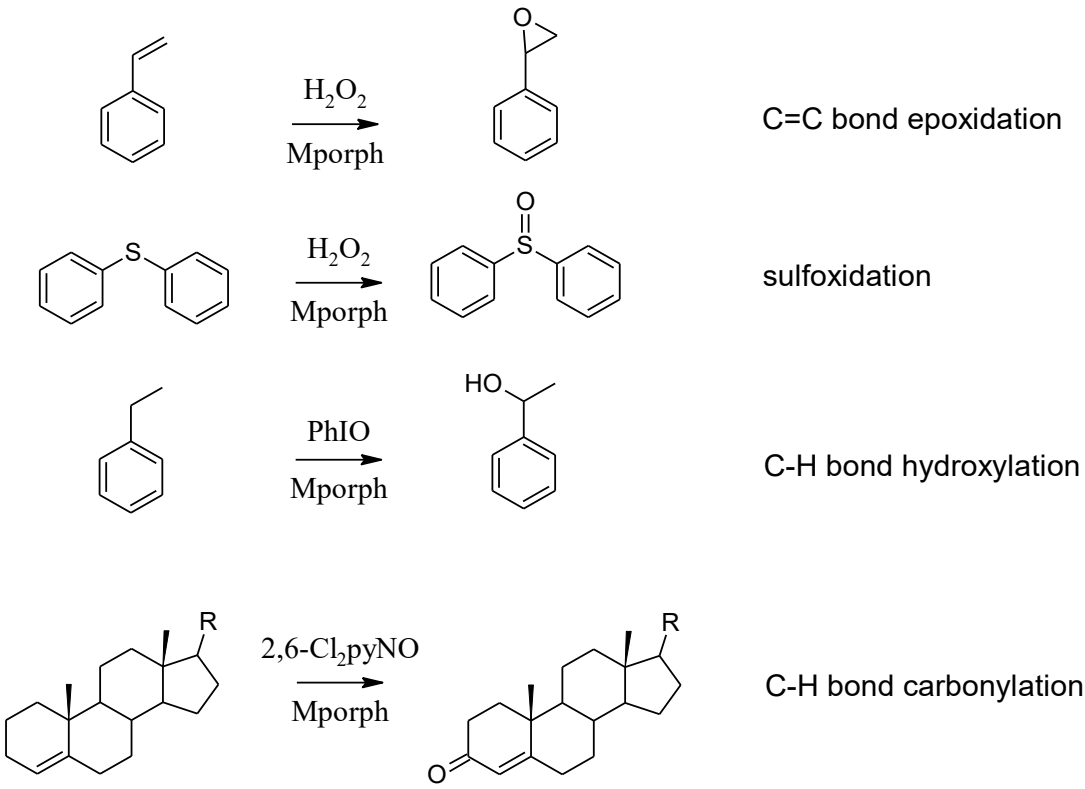

Figure 17. Examples of reactions catalysed by metalloporphyrins incorporated in porous frameworks (Mporph stands for a metalloporphyrin).

As described above, porphyrin is a luminescent molecule which can be quenched by π-π stacking with other aromatic systems, so that in the presence of specific organic molecules the luminescence diminishes. This quenching can be used for a detection of nitroaromatic explosives.[81] Another possible application of porphyrin porous frameworks originates from the photosensitizing properties of porphyrins. Singlet oxygen produced *in situ* by a porous framework is applicable for the oxidation of mustard gas, (bis(2-chloroethyl)sulphide), to the corresponding sulfoxide[82] or in PDT, however, the highest efficiency of PDT agents is achieved when they are internalized by cells. For this reason, porphyrin porous frameworks for PDT are synthesized in nanoscale with defined particle sizes.[83] Porphyrin porous frameworks can be prepared in the form of thin films, which can be used as antimicrobial coatings.[84] MOFs are the most studied group of porous frameworks in terms of the application for PDT, mainly because of the easiest way to control the final particle size.[85] On the other hand, the limitations of the majority of porphyrin MOFs is the presence of OH^- ligands in the SBUs, which are known to quench $O_2(^1\Delta_g)$, and the proximity of heavy atoms. The latest studies indicate that these limitations can be partially overcome by a postsynthetic modification, e.g., modification of a zirconium-based MOF PCN-222 with diphenylphosphinic acid which leads to the replacement of OH^- ligands on the SBUs for

diphenylphosphinate ions.[86] The presence of phosphinates in the structure of MOFs does not only increase the yield of $O_2(^1\Delta_g)$, but it also improves the stability of the material in aqueous environment.[30] Therefore, a MOF based on a porphyrin phosphinic acid might be a potent $O_2(^1\Delta_g)$ photosensitizer with high stability in aqueous environment.

2 Aims of the work

Porphyrins are molecules with high chemical stability and good quantum yields of singlet oxygen formation. However, the strong intermolecular interactions in certain environments cause the loss of their photosensitizing properties. The previously studied incorporation of porphyrin molecules into non-porous hybrid materials is not an effective approach due to the enhanced quenching of produced singlet oxygen and poor permeability for gases. Porous frameworks were suggested as a solution of these obstacles. Although several MOFs have been already studied as potential photosensitizers of singlet oxygen, their photosensitizing efficacy is rather low. The aim of the work is to prepare new non-metallic porous frameworks (COFs and CMPs), investigate their photosensitizing properties, and compare them with the efficacy of porphyrinic MOFs. Another possible approach involves novel porphyrin containing phosphinic acid-based MOFs, which are expected to be better photosensitizers than commonly used MOFs due to the absence of –OH groups in the SBUs and higher stability in aqueous environment. The objectives of the thesis are formulated as follows:

1. Synthesis of new porphyrin-based COFs and CMPs, employing different types of building blocks bonding (C = N or C – C) and topologies (2D, 3D), and tuning the distance between the porphyrin units. Characterization of prepared materials (IR and MAS-NMR spectroscopy, XRD, sorption measurements).
2. Delineation of morphology, spectral and photophysical properties of newly synthesized materials including absorption and fluorescence properties, kinetics of excited states, singlet oxygen productivity. These data can allow to draw the structure – properties relationship and to compare photosensitization efficacy of COFs and CMPs with porphyrinic MOFs.
3. Construction of antimicrobial coatings based on porous frameworks producing singlet oxygen upon irradiation, testing their bactericidal activity on inhibition of bacterial biofilms growth.
4. Synthesis of porphyrin phosphinic acids, which can serve as either linker molecules for new MOFs or agents for a postsynthetic modification of MOFs. The photophysical and photobiological properties of these novel compounds will be described.

3 Results and discussion

3.1 Porphyrin-based CMPs and COFs

Appendix I describes the synthesis, physicochemical, and photophysical properties of a series of porphyrin-based conjugated microporous polymers with either 2D or 3D topology.[87] The objective was to elucidate the relationship between the chemical surrounding of the porphyrin moiety and the photophysical characteristics of the resulting materials.

For the preparation of porphyrin CMPs, a palladium-catalysed Suzuki coupling reaction was employed. For the reaction, two types of precursors were used: an aryl bromide with two or more Br atoms and a boronic acid or alternatively, its ester also containing two or more boronic groups (Scheme 1). The precursors were either commercially available or they were synthesized according to Scheme 2. The reactions were usually done at 100 °C under inert atmosphere for 24 h. The resulting solid products were collected by filtration, washed thoroughly by various organic solvents, and furtherly purified by Soxhlet extraction. For the preparation of CMPs with 2D topology (2D-TPP_CMP and 2D-PdTPP_CMP), a combination of 5,10,15,20-tetrasubstituted tetraphenylporphyrin (TPP) and 1,4-disubstituted benzene was used, similarly to the published procedure.[79] On the other hand, for the preparation of 3D CMPs, 5,15-disubstituted tetraphenylporphyrin or diphenylporphyrin (DPP) and tetrasubstituted tetraphenylmethane precursors were employed. For both 2D and 3D CMPs, either non-metallated porphyrins or their Pd(II) complexes were utilized. 3D CMPs materials, containing either 5,10,15,20-tetraphenylporphyrin (3D-TPP_CMP and 3D-PdTPP_CMP) or 10,20-diphenylporphyrin (3D-DPP_CMP) moieties, were synthesised to investigate the effect of porphyrin-porphyrin distance in the structure on the properties of resulting materials.

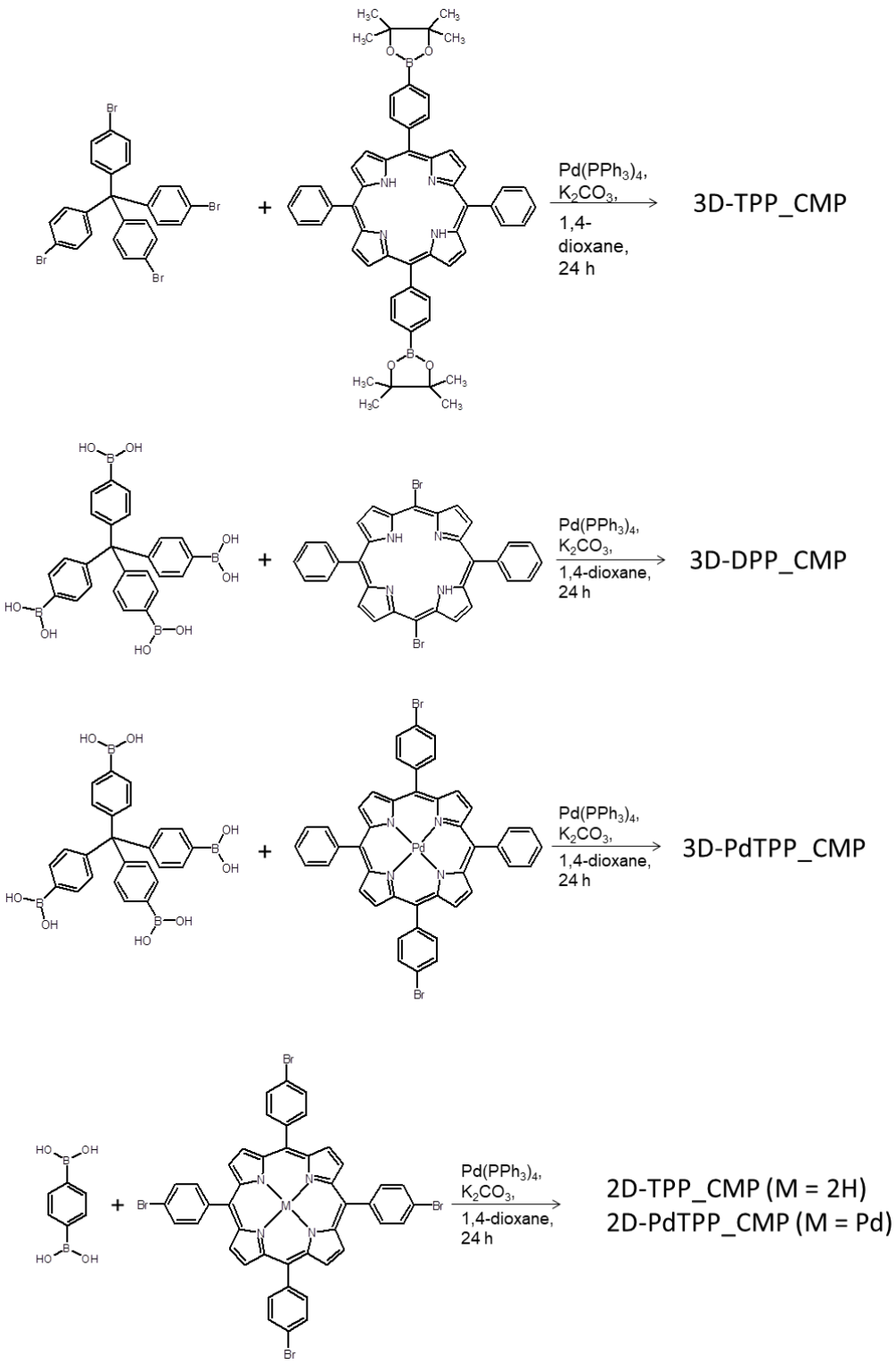

Scheme 1. Synthetic route to preparation of the porphyrin-based CMPs.

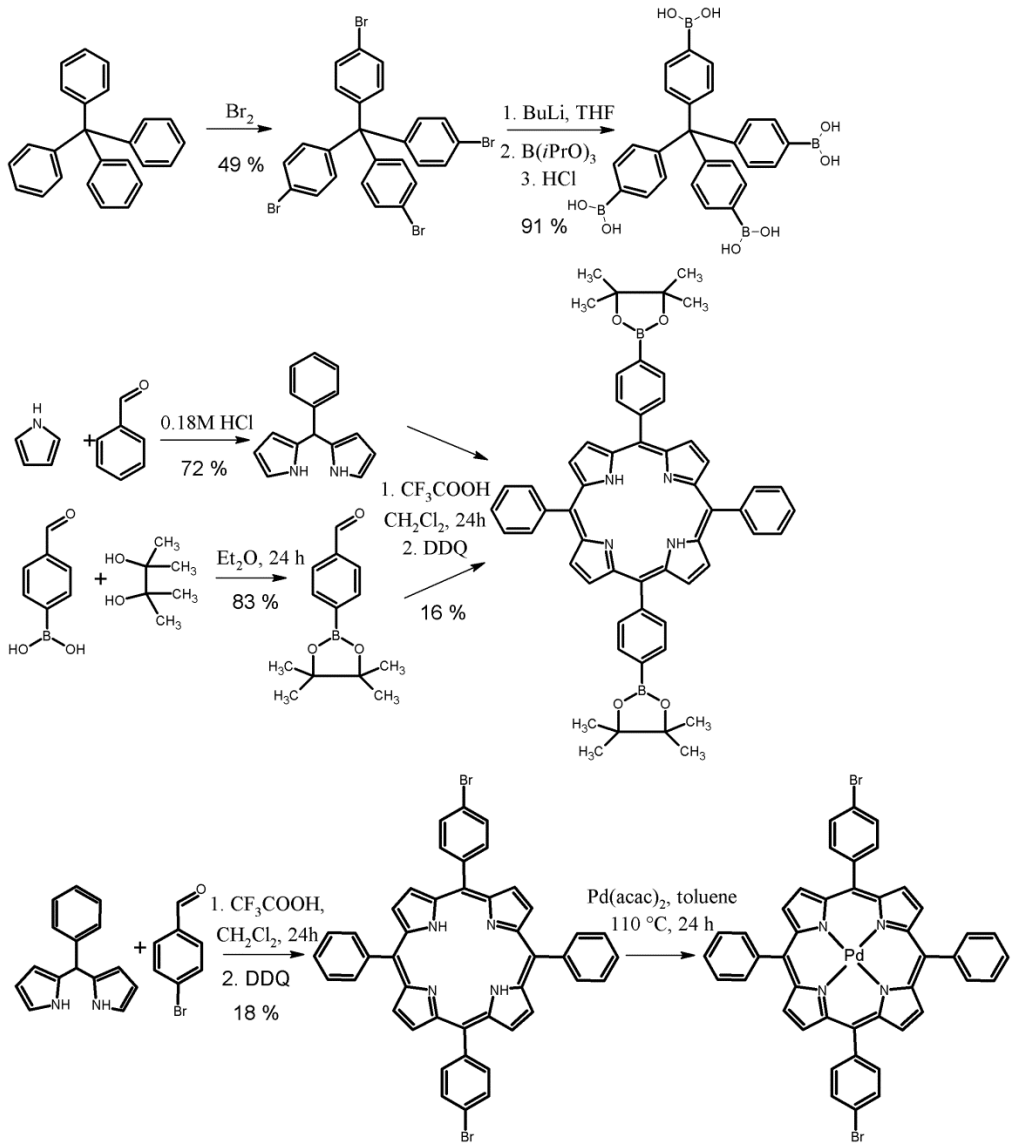

Scheme 2. Synthesis of the precursors for porphyrin-based CMPs (detail procedures are given in Appendix I). DDQ stands for 2,3-dichloro-5,6-dicyano-1,4-benzoquinone.

The synthesis of porphyrin-based COFs is described in Appendix II.[88] The preparation procedure involved an acid-catalysed Schiff condensation, starting from a primary amine and an aldehyde (Scheme 3). This procedure was developed earlier for the preparation of porphyrin-based COF-366,[49] hereafter denoted 2D-TPP_COF. Analogously, porphyrin containing 3D COFs were prepared from tetrakis(4-aminophenyl)methane and 5,15-bis(4-formylphenyl)-10,20-diphenylporphyrin (3D-TPP_COF) or its Pd(II) complex (3D-PdTPP_COF). Synthesis of the porphyrins is depicted in Scheme 4. The materials were purified by Soxhlet extraction and characterized by IR and ^{13}C MAS-NMR spectroscopy (MAS = magic angle spinning). Adsorption properties of the materials were studied as well as their photophysical characteristics. Then, porphyrin-based COFs were successfully used for

preparation of antibacterial coatings, which were tested for inhibition of bacterial biofilms growth.

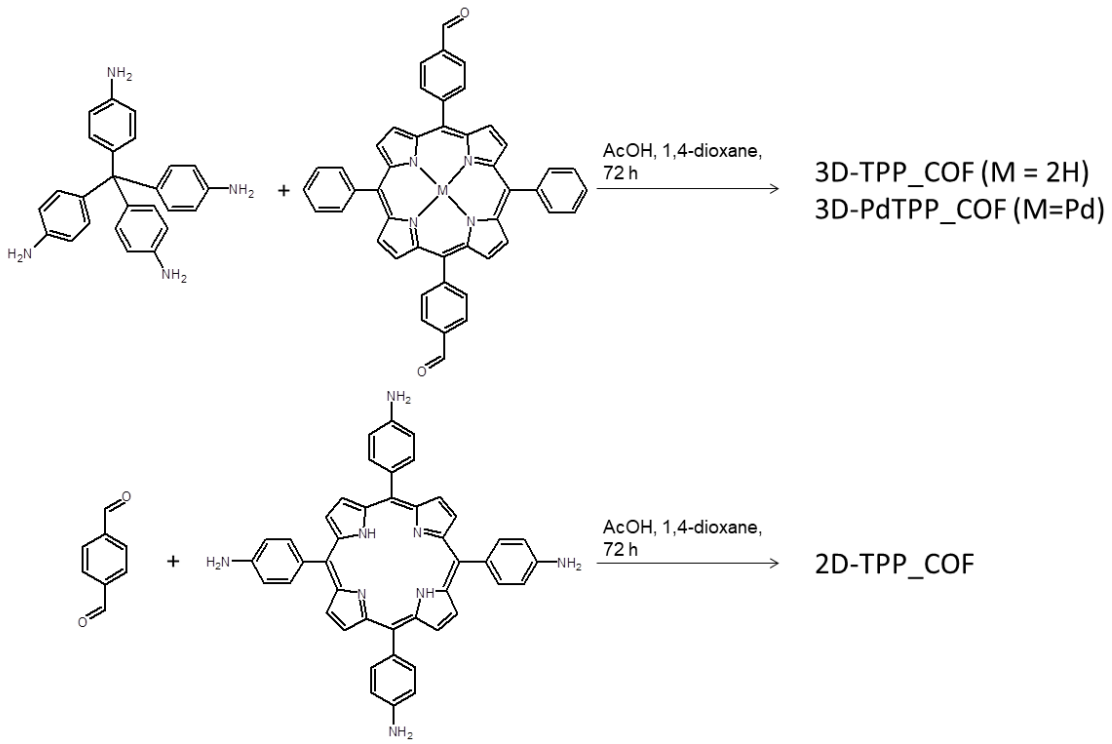

Scheme 3. Synthetic route to preparation of the porphyrin-based COFs.

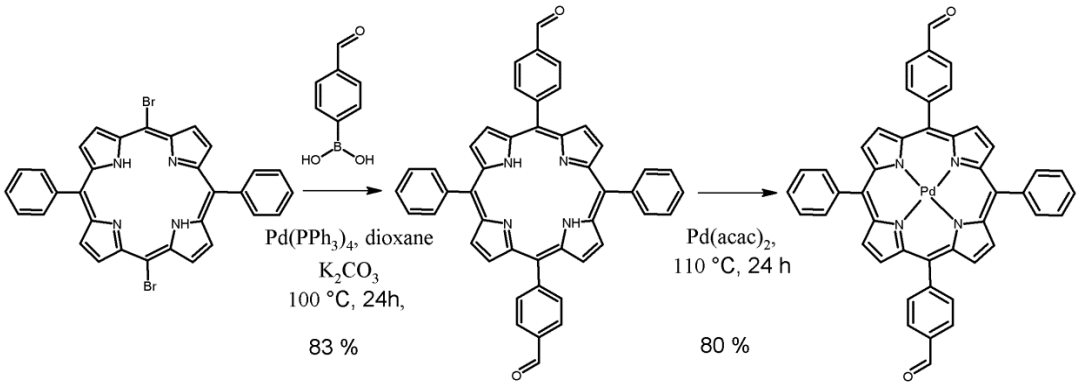

Scheme 4. Synthesis of the precursors for porphyrin-based COFs (detail procedures are given in Appendix II).

3.1.1 Structural characterisation

The prepared CMPs and COFs were characterised by IR and ^{13}C MAS-NMR spectroscopy. The IR spectra of the CMPs, which are depicted in Figure 18, reveal vibrational peaks characteristic for porphyrins: stretching aromatic C–H vibrations in the range of 3022 – 3054 cm^{-1}, a sharp peak at 794 – 798 cm^{-1} corresponding to pyrrole ring vibration, and an N–H

stretching vibration at 3313 cm^{-1}, which disappears in palladium containing polymers 2D-PdTPP_CMP and 3D-PdTPP_CMP.

The structure of COFs is composed of porphyrin building blocks connected via C=N bonds, which have a characteristic stretching vibration at 1620 cm^{-1}, see Figure 19. The materials also contain residual aldehyde and NH_2 groups. The aldehyde groups can be documented by the peaks at 1700 cm^{-1}, and peaks at 3380 and 3470 cm^{-1} belong to stretching N–H vibrations of the residual NH_2 groups.

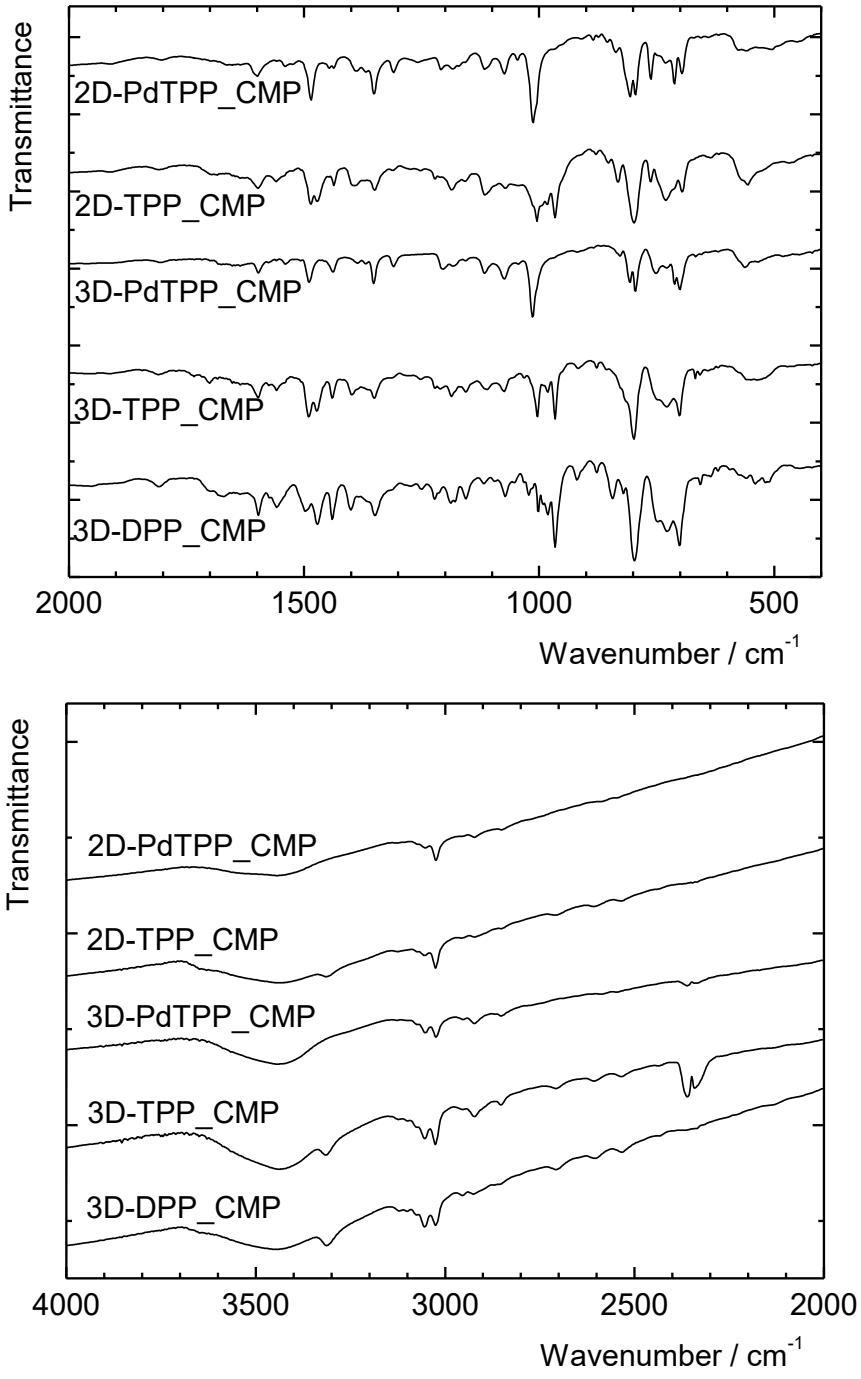

Figure 18. FTIR spectra of porphyrin-based CMPs.

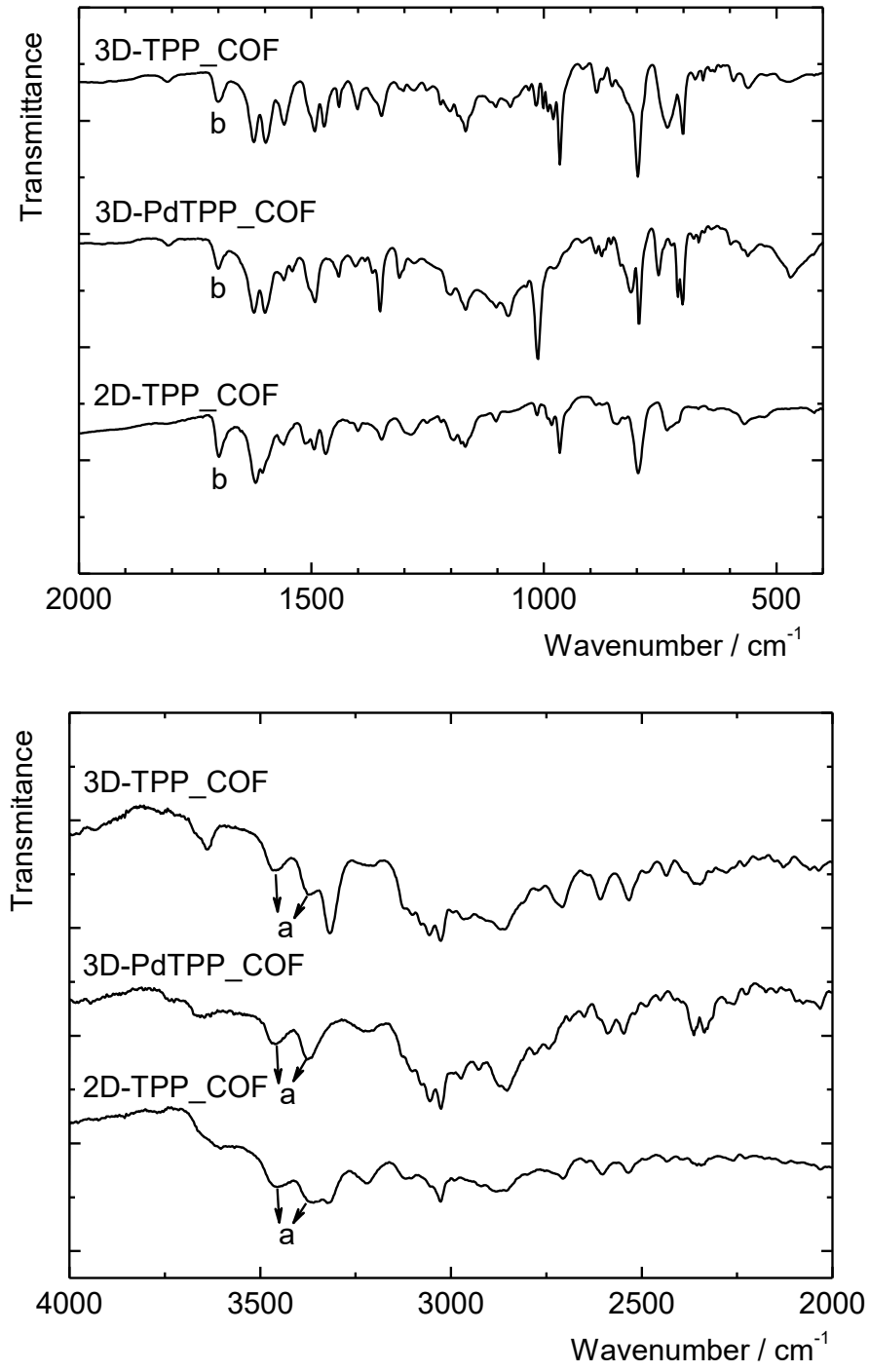

Figure 19. IR spectra of the COFs: region 400 – 2000 cm^{-1} was measured in KBr pellets and the region 2000 – 4000 cm^{-1} was measured with a diffuse reflection accessory; residual amino (a) and aldehyde (b) groups are labelled.

The ^{13}C MAS-NMR spectra (Figure 20 and 21) reveal signals typical for porphyrins: tertiary and quaternary pyrrole carbon atoms can be found in the range between 120 – 150 ppm,

intensive peaks at 141 ppm belong to the quaternary phenylene and *meso*-carbon atoms of the porphyrin rings, and signals of tertiary phenylene carbon atoms are at 127 ppm. In the case of 3D materials, the spectra show also peaks of quaternary carbons and tertiary phenylene carbon atoms of tetraphenyl methane at 65 and 131 ppm, respectively. The spectra of porphyrin-based COFs contain additional peaks at 158 ppm attributed to imine carbons from the linking groups. In the case of 2D-TPP_COF, a peak of the residual aldehyde groups at 190 ppm is also distinguishable.

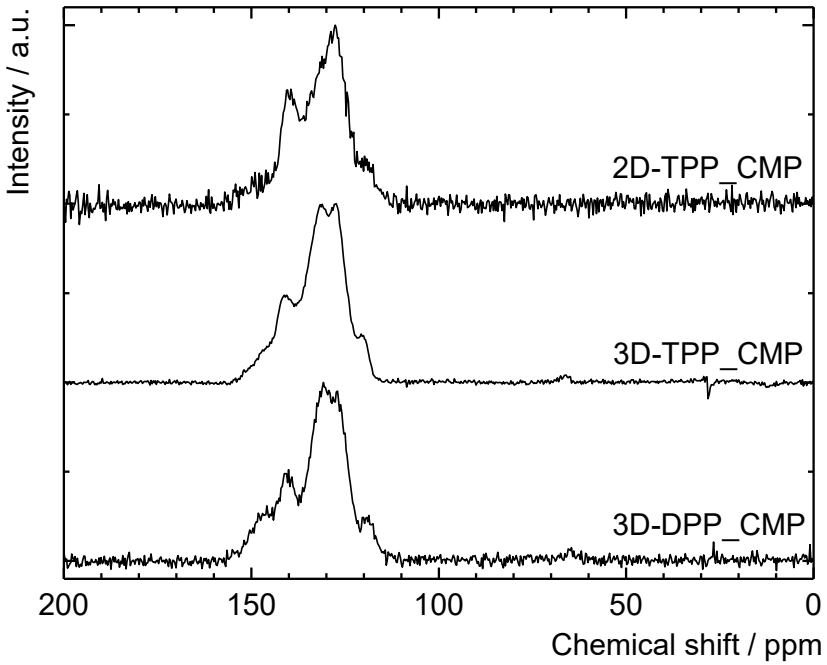

Figure 20. ^{13}C MAS-NMR spectra of porphyrin-based CMPs.

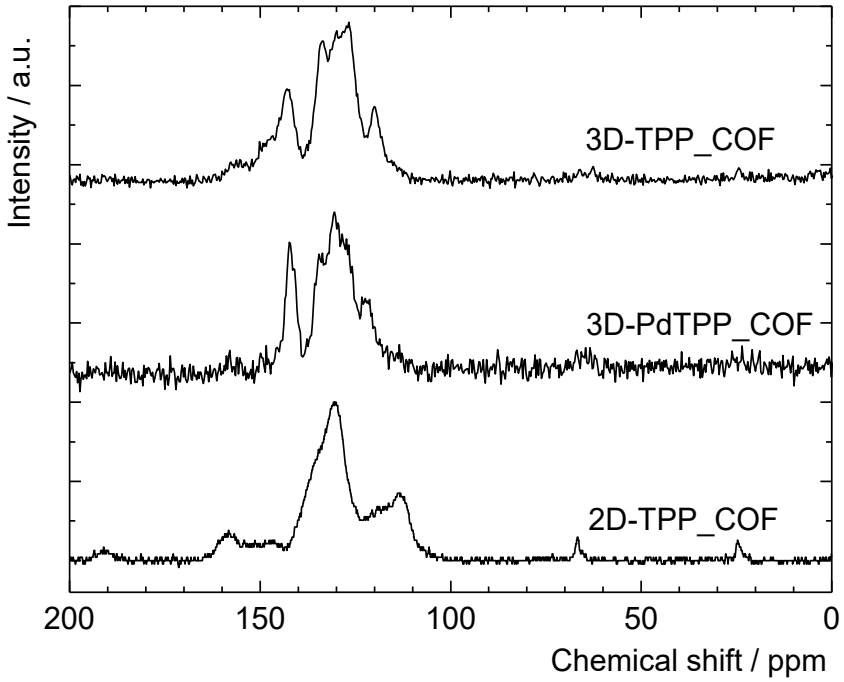

Figure 21. ^{13}C MAS-NMR spectra of porphyrin-based COFs.

3.1.2 Adsorption properties

To characterize the porous nature of the prepared materials, measurement of N_2 sorption at 77 K was performed. The CMPs considerably adsorb at low pressures ($P/P_0 < 0.1$), indicating their microporous nature. The adsorption isotherms show very broad hysteresis loop, the desorption branch is parallel to the adsorption branch joining it at low relative pressure of approximately 0.01. Desorption at such low pressures was so slow that it took tens of hours to achieve the equilibrium state. This can be a consequence of the elastic nature of the CMPs.

When pore characteristics of particular CMPs are compared (Table 1), 3D-DPP_CMP contains narrower pores than 3D-TPP_CMP. When diphenylporphyrin building blocks are replaced for tetraphenylporphyrin, the pore size grows to 2.1 nm (3D-DPP_CMP). On the other hand, total pore volume decreased from 624 to 353 $m^2\ g^{-1}$ since wider pores enable incorporation of oligomers and interpenetration of the structure. 2D-TPP_CMP contains micropores with a diameter of approximately 2.0 nm. This value well corresponds to the expected pore size calculated as a distance between neighbouring porphyrin units (approx. 2 nm).[79]

In the case of Pd(II) porphyrin-based materials, significantly lower porosity in comparison with free porphyrin-containing CMPs (3D-PdTPP_CMP) or no porosity was measured. The reason probably is the less flexible structure of these materials leading to pore blocking.

Table 1. Textural parameters of the investigated CMPs.

Sample	S_{BET} / m^2g^{-1}	$(P/P_0)_{val}$	V_{pore} / cm^3g^{-1}	Pore width/nm
2D-TPP_CMP	443	0.05-0.10	0.18	2.0
2D-PdTPP_CMP	37	0.05-0.20	-	nonporous
3D-TPP_CMP	353	0.05-0.25	0.20	2.1
3D-PdTPP_CMP	112	0.05-0.25	0.043	1.4
3D-DPP_CMP	624	0.05-0.10	0.29	< 1.8

In contrast with porphyrin-based CMPs, the investigated 3D COFs contain both mesopores and micropores and their total surface area is significantly lower (Table 2), which is probably caused by interpenetration of their diamond-like structure. The complexation of Pd(II) in the case of 3D-PdTPP_COF leads to the disappearance of microporosity. The distribution of mesopores is in both cases very broad without any characteristic maxima. For this reason, occurrence of mesopores can be attributed to structural defects rather than to organized structural voids. 2D-TPP_COF contains mesopores with ca. 2 nm in diameter, which is in good agreement with the expected distance between neighbouring porphyrin units and the results reported in literature for COF-366.[49]

Table 2. Texture parameters of the investigated COFs.[a]

Sample	Texture	S_{BET} / m^2g^{-1}	V_{micro}[b] / cm^3g^{-1}	S_{micro}[b] / m^2g^{-1}	V_{meso}[b] / cm^3g^{-1}	S_{meso}[b] / m^2g^{-1}	D_{max} / nm	S_{ext} / m^2g^{-1}
3D-TPP_COF	micro-meso bimodal	83	0.02	43	0.08	35	1.2, 9	5
3D-PdTPP_COF	mesoporous	50	0	0	0.12	50	7-8	very small
2D-TPP_COF	microporous	475	0.20	475	0	0	~ 2	very small

[a] S_{BET} stands for the BET surface area; V is the pore volume of micropores or mesopores determined by the Broekhoff-de Boer t-plot method; D_{max} is the pore width determined by the NLDFT method, corresponding to the maximum/maxima of the pore size distribution; S_{ext} is the external surface. [b] Determined by the Broekhoff-de Boer t-plot method.

3.1.3 Photophysical properties

Characterization of photophysical properties involved measurement of absorption spectra, fluorescence spectra, time-resolved fluorescence, and phosphorescence of $O_2(^1\Delta_g)$. In the case of porphyrin COFs, other photophysical characteristics, such as lifetimes of triplet states and $O_2(^1\Delta_g)$, or quantum yields of $O_2(^1\Delta_g)$ formation, were also determined.

The absorption spectra of the CMPs depicted in Figure 22 and 23 show Soret bands, which are in comparison with monomeric porphyrin in solution red-shifted to 440 – 450 nm and significantly broadened as a consequence of the stacking of porphyrin units in the materials. The Soret bands reveal shoulders at approximately 415 nm belonging to the monomeric form of porphyrin. The Q-bands are also red-shifted, this is most pronounced in the case of 2D-TPP_CMP with the strongest interaction between porphyrin units.

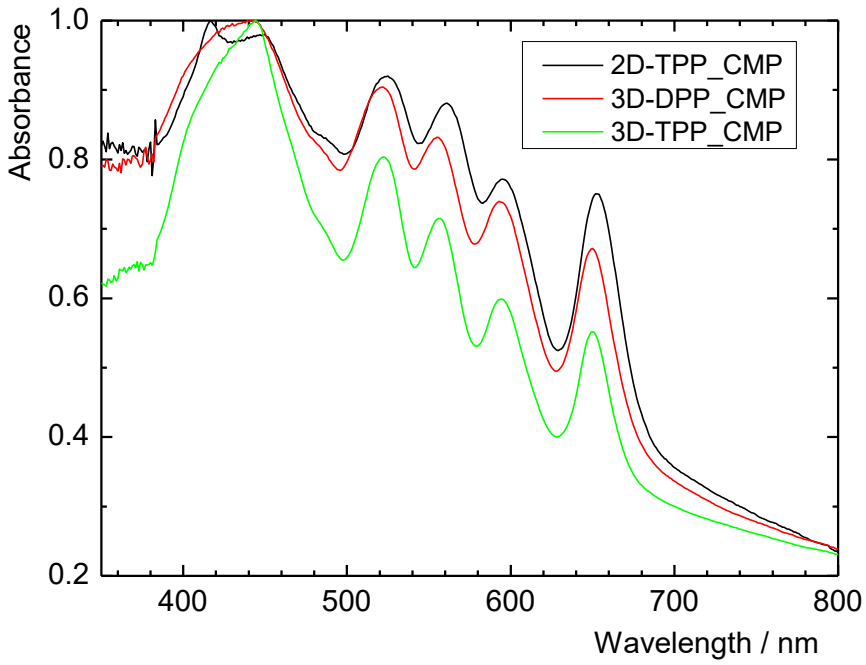

Figure 22. Normalized absorption spectra of the CMPs containing non-metallated porphyrin building units measured in acetonitrile dispersions.

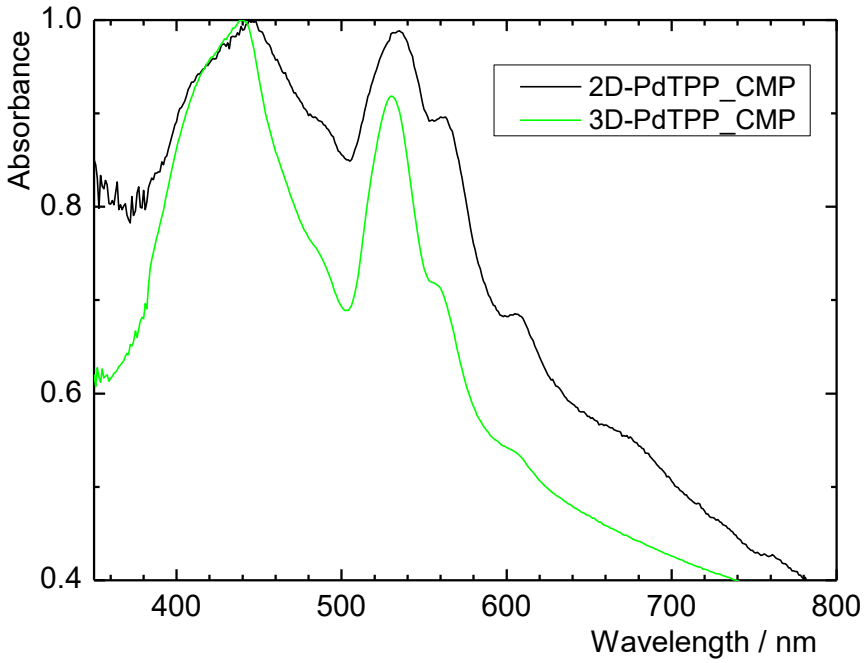

Figure 23. Normalized absorption spectra of the CMPs containing Pd(II) porphyrin building units measured in acetonitrile dispersions.

In contrast with the CMPs, the absorption spectra of porphyrin-based COFs (Figure 24) reveal sharp bands with a negligible red shift in comparison with TPP in solution. This feature evidences efficient suppression of porphyrin stacking in the structure of COFs, especially in the case of 3D COFs.

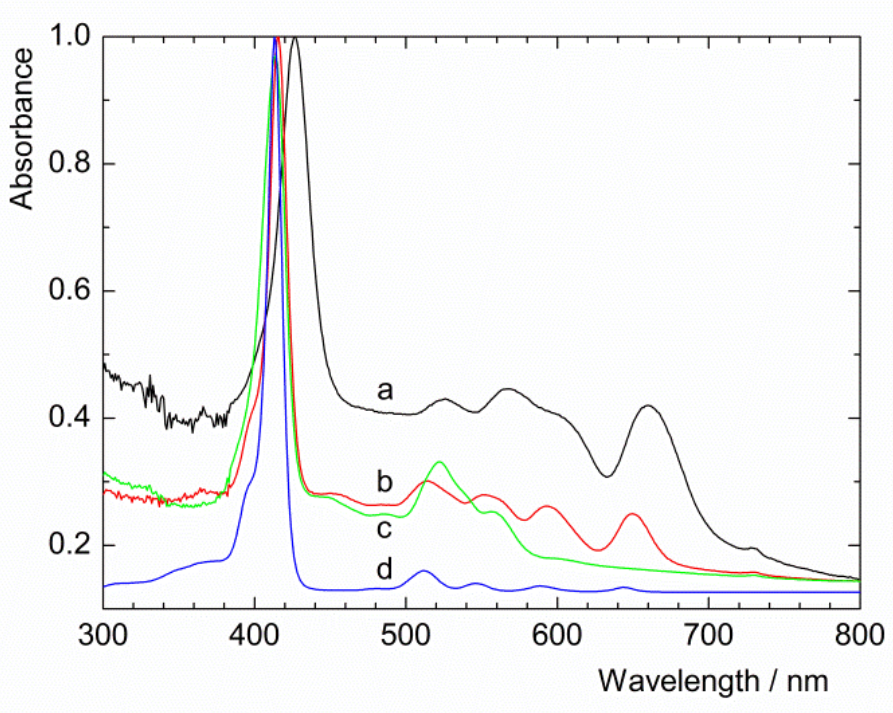

Figure 24. Normalized absorption spectra of 2D-TPP_COF (a), 3D-TPP_COF (b), 3D-PdTPP_COF (c) dispersed in acetonitrile compared with the spectrum of TPP in acetonitrile (d).

The fluorescence emission spectra of non-metallic porphyrin containing CMPs (Figure 25), show differences between monomeric TPP and corresponding CMPs. Whereas the Q(0,0) and Q(0,1) emission bands of TPP are at 647 and 714 nm, in the case of CMPs, these bands are significantly broadened and red-shifted to 658 – 666 and 720 – 721 nm, respectively. The fluorescence lifetimes of 2D-TPP_CMP, 3D-DPP_CMP, and 3D-TPP_CMP are 1.7, 0.8, and 0.6 ns, respectively, which are lower values than 9.2 nm for TPP in solution. The red shift of fluorescence bands and shortening of fluorescence lifetime reflect partial stacking of the porphyrin units in the structure of CMPs.

The emission spectrum of the CMP made of Pd(II) porphyrin (3D-PdTPP_CMP) depicted in Figure 26 reveals fluorescence bands at 575 and 613 nm and phosphorescence bands at 710 and 785 nm. Analysis of a phosphorescence decay by a biexponential function provides a phosphorescence lifetime of 120 μs, which is the same order of magnitude as the corresponding lifetime of monomeric porphyrin in solution (Pd(II)TPPS has phosphorescence lifetime of 297 μs in water). The intensity of fluorescence bands is not affected by the presence of oxygen, whereas the phosphorescence intensity strongly depends on the oxygen concentration. In general, the quenching of phosphorescence by oxygen is a consequence of

the energy transfer from porphyrin triplet states to O_2 molecules resulting in the formation of $O_2(^1\Delta_g)$. In the case of 2D-PdTPP_CMP (see Figure 27), the phosphorescence is diminished even in the absence of dissolved oxygen. This material, which consists of closely stacked sheets of polymerized porphyrin and does not have porosity, evidently contains highly aggregated porphyrin units resulting in efficient self-quenching of the triplet states.

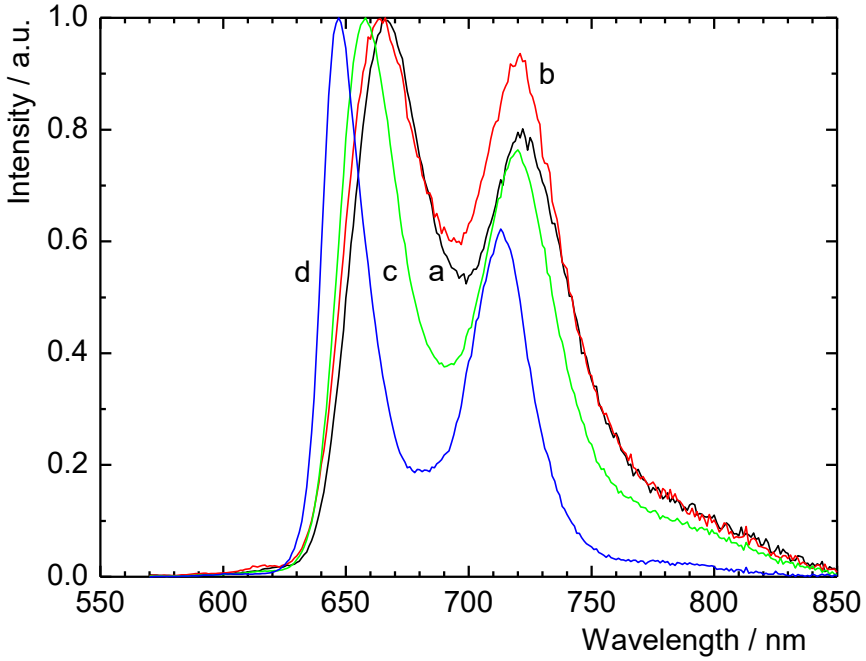

Figure 25. Normalized fluorescence emission spectra of 2D-TPP_CMP (a), 3D-DPP _CMP (b), and 3D-TPP_CMP (c) in acetonitrile dispersions (λ_{exc} = 520 nm) compared with that of 5,10,15,20-tetraphenylporphyrin in acetonitrile (d) (λ_{exc} = 510 nm).

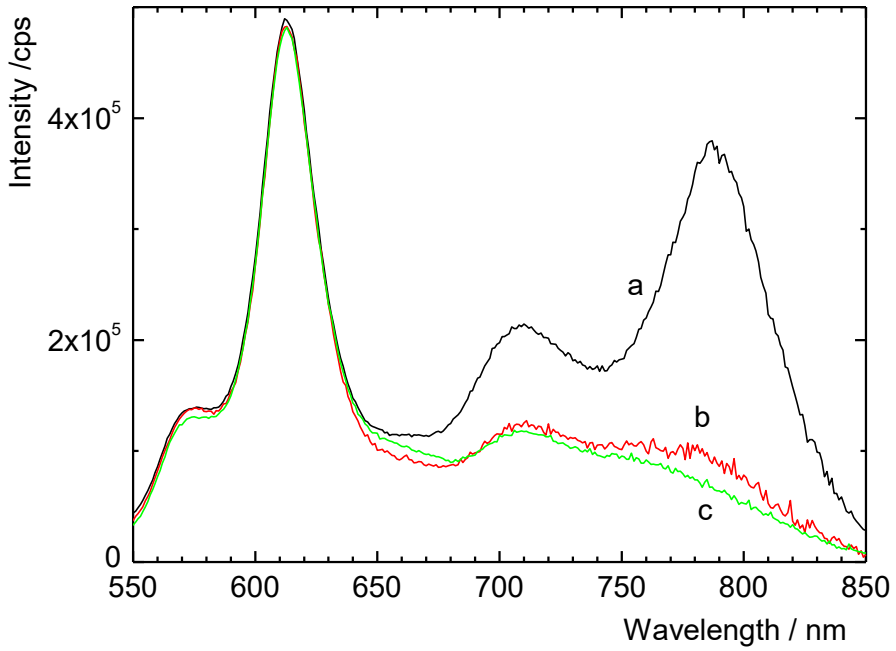

Figure 26. Luminescence emission spectra of 3D-PdTPP_CMP dispersions in acetonitrile in the absence of oxygen (a), saturated by air (b) or oxygen (c). The excitation wavelength was 440 nm.

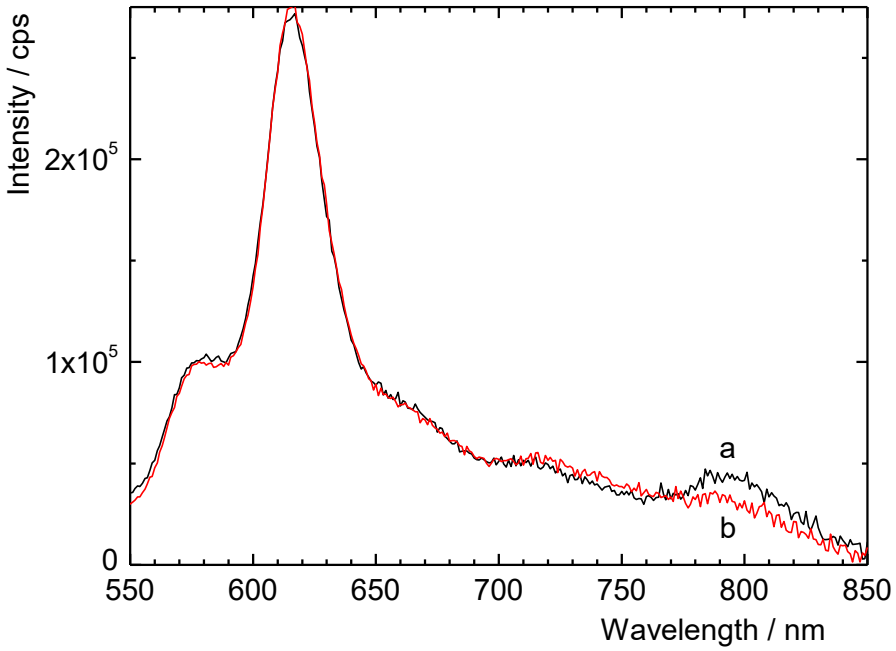

Figure 27. Luminescence emission spectra of 2D-PdTPP_CMP dispersions in acetonitrile in the absence of oxygen (a), or saturated by air (b). The excitation wavelength was 440 nm.

The fluorescence spectra of the investigated COFs depicted in Figure 28 show significant red shift of Q(0,0) and Q(0,1) fluorescence bands, even more pronounced than in the case of porphyrin-based CMPs. The fluorescence decay curves of porphyrin COFs are biphasic with two components: 1.94 (9%) and 11.9 (91%) ns for 3D-TPP_COF, and ≤ 0.4 (10%) and 9.02 (90%) ns for 2D-TPP_COF. The fluorescence lifetimes are shorter than that for TPP (9.20 ns), however, they are longer than those of porphyrin CMPs. In agreement with findings described above, this fact can be also attributed to lesser extent of stacking of the porphyrin moieties in the structure of COFs when compared with the CMPs.

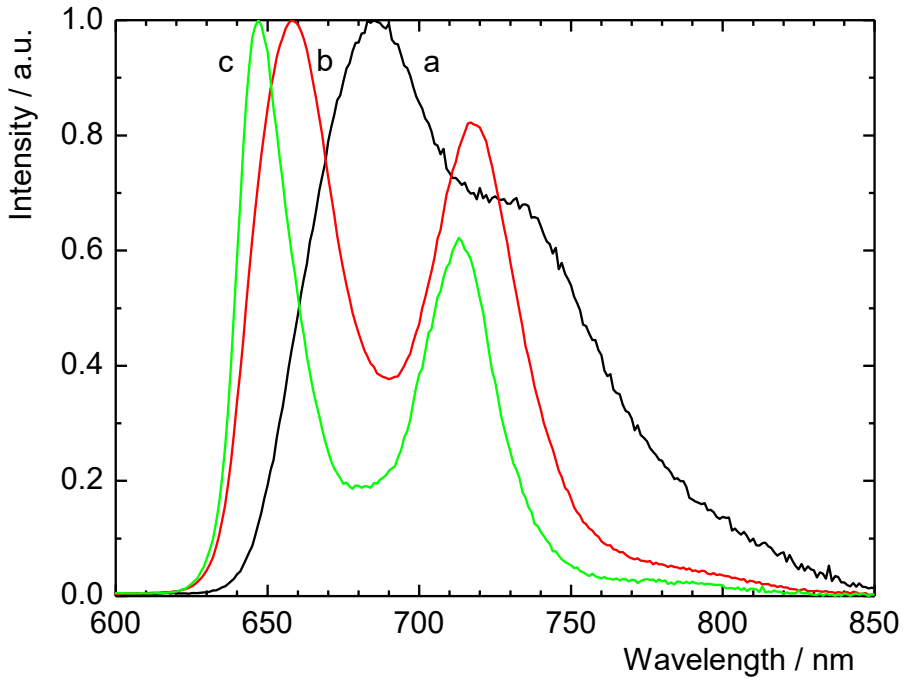

Figure 28. Normalized fluorescence emission spectra of 2D-TPP_COF (a) and 3D-TPP_COF (b) dispersed in acetonitrile compared with that of TPP (c).

The emission spectra of 3D-PdTPP_COF reveal a fluorescence band at 609 nm (Figure 29). In the absence of oxygen, the fluorescence band is preserved and is accompanied by the appearance of phosphorescence bands at 699 and approximately 765 nm. The phosphorescence lifetime, which corresponds to the lifetime of the triplet states (see Table 3), is 200 μs in the oxygen-free environment.

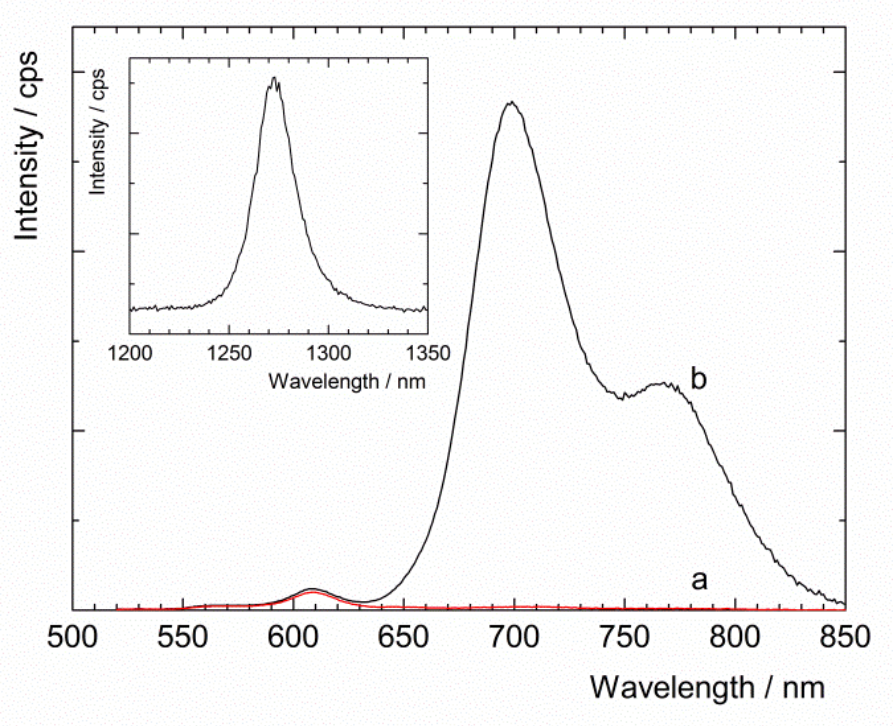

Figure 29. Luminescence emission spectra of 3D-PdTPP_COF dispersions in acetonitrile saturated by air (a) and in the absence of oxygen (b). The excitation wavelength was 410 nm. Inset: Corresponding phosphorescence band of produced $O_2(^1\Delta_g)$ upon excitation at 520 nm in air-saturated acetonitrile.

One of the possible methods to prove the $O_2(^1\Delta_g)$ formation is the observation of its characteristic phosphorescence at 1270 nm. This method was also applied in the case of the prepared CMPs. The material dispersions were irradiated at 420 nm, in the region of the most intensive absorption band of porphyrin, and corresponding emission of $O_2(^1\Delta_g)$ in the NIR region was recorded. For all types of porphyrin CMPs, phosphorescence of $O_2(^1\Delta_g)$ was observed in oxygen- or air-saturated environment. When oxygen was removed from the dispersions by bubbling with argon, no phosphorescence was observed in the case of 3D-TPP_CMP, 3D-PdTPP_CMP, and 2D-PdTPP_CMP (Figure 30), whereas highly porous CMPs (3D-DPP_CMP and 2D-TPP_CMP shown in Figure 31) did produce $O_2(^1\Delta_g)$ even after the removal of oxygen from the solvent because oxygen remained trapped in the microporous structures.

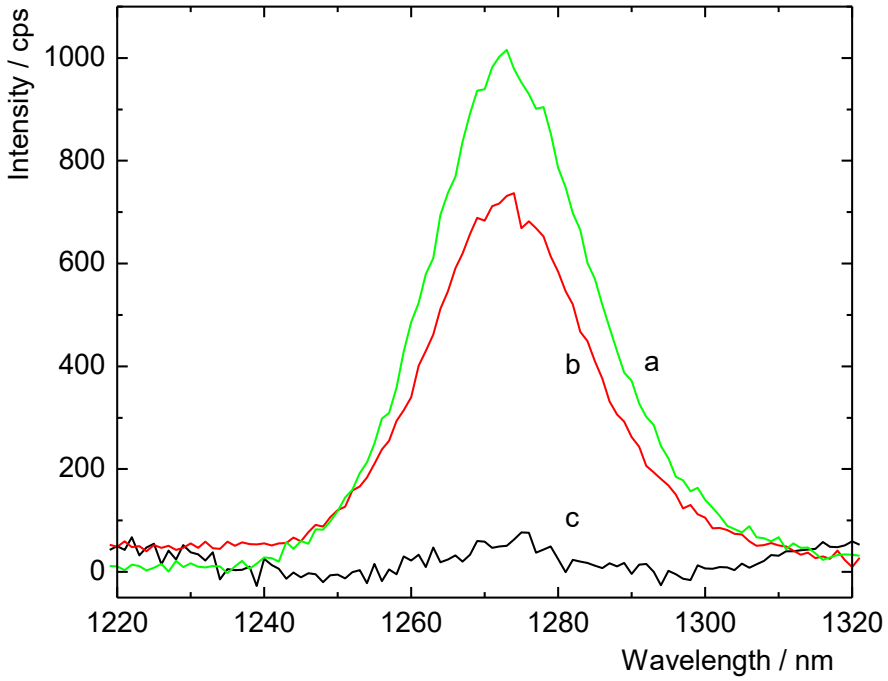

Figure 30. Phosphorescence emission spectra of photosensitized $O_2(^1\Delta_g)$ produced in acetonitrile dispersions of 3D-PdTPP_CMP in oxygen (a), air (b), and argon atmosphere (c) upon excitation at 420 nm.

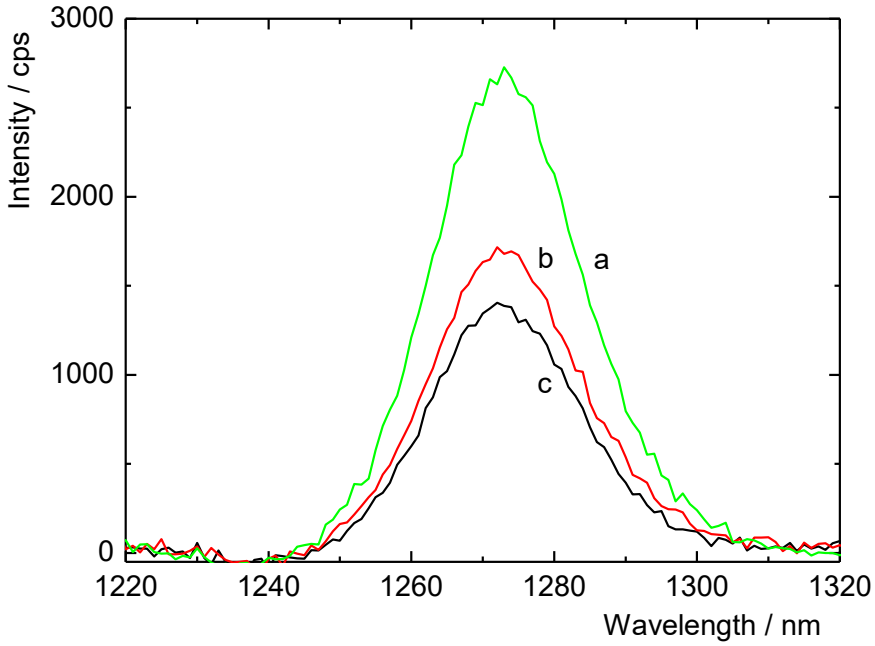

Figure 31. Phosphorescence emission spectra of photosensitized $O_2(^1\Delta_g)$ produced in acetonitrile dispersions of 2D-TPP_CMP in oxygen (a), air (b), and argon atmosphere (c) upon excitation at 420 nm.

Since the porphyrin COFs have absorption and emission characteristics similar to the monomeric TPP in solution, the kinetics of the triplet states quenching by oxygen, $O_2(^1\Delta_g)$ lifetimes, and quantum yields of $O_2(^1\Delta_g)$ formation can be also measured. The triplet state lifetimes of non-metallic porphyrin COFs, determined by transient absorption spectroscopy, are longer than the lifetime of monomeric TPP in solution (Table 3). This result points to the suppression of non-radiative processes due to the limited interaction of the porphyrin moieties with the solvent. The triplet states of porphyrins in COFs efficiently interact with molecular oxygen, which is documented by the high fractions of the triplet states quenched by oxygen and high values of the bimolecular rate constants of quenching of the triplet states by molecular oxygen, k_{O2}, obtained using the Stern-Volmer equation: $1/\tau_T^{air} = 1/\tau_{T0} + k_{O2}[O_2]$, where τ_T^{air} is the triplet state lifetime in air atmosphere, τ_{T0} is the triplet state lifetime in oxygen-free environment, and $[O_2]$ is the solubility of oxygen in acetonitrile (2.42 mM) (Table 3).

Similarly to the CMPs, all three porphyrin COFs produce $O_2(^1\Delta_g)$ as documented by the characteristic phosphorescence of $O_2(^1\Delta_g)$ at approximately 1270 nm. The analysis of kinetic profiles of $O_2(^1\Delta_g)$ phosphorescence provides corresponding lifetimes for each material. The lifetimes correspond to the $O_2(^1\Delta_g)$ lifetime in pure acetonitrile (75 μs),[89] which documents negligible interaction of COFs with thus produced $O_2(^1\Delta_g)$.

Table 3. Photophysical properties of the COF dispersions in acetonitrile.[a]

	Triplet states			$O_2(^1\Delta_g)$	
	τ_{T0} / μs	k_{O2} / $M^{-1}s^{-1}$	f_T^{air}	Φ_Δ	τ_Δ / μs
3D-TPP_COF	490	1.4×10^9	>0.999	0.58	75
3D-PdTPP_COF	200	1.3×10^9	0.998	0.56	78
2D-TPP_COF	460	1.9×10^9	>0.999	0.67	77
TPP	68	1.6×10^9	0.997	0.60[b]	75

[a] τ_{T0} stands for the lifetime of the porphyrin triplet states in argon-saturated acetonitrile; k_{O2} is the bimolecular rate constant of the triplet state quenching by oxygen; $f_T^{air} = 1-\tau_T/\tau_{T0}$, i.e., it is the fraction of the triplet states produced quenched by oxygen in air-saturated acetonitrile; Φ_Δ is the quantum yield of singlet oxygen formation; τ_Δ is the lifetime of $O_2(^1\Delta_g)$. [b] Literature value, ref [90].

3.1.4 Singlet oxygen productivity

The efficacy of $O_2(^1\Delta_g)$ production can be quantified using $O_2(^1\Delta_g)$-mediated reactions. Then, the $O_2(^1\Delta_g)$ productivity can be estimated via the measurement of a yield of these reactions. In this respect, $O_2(^1\Delta_g)$-mediated oxidation of 9,10-diphenylathracene to the corresponding endoperoxide is a suitable reaction system because it offers high selectivity, thermal stability of the substrate, and the product formation and its kinetics can be followed by UV-vis spectroscopy (Scheme 5).

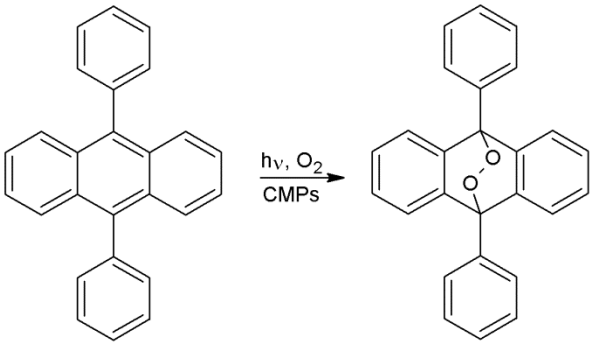

Scheme 5. Reaction of $O_2(^1\Delta_g)$ with 9,10-diphenylanthracene.

The reaction curves of 9,10-diphenylanthracene oxidation are shown in Figure 32. Since during the blank experiments performed in the absence of CMPs or COFs the concentration of 9,10-diphenylathracene did not change, the decreasing absorbance of 9,10-diphenylathracene can be fully attributed to its reaction with $O_2(^1\Delta_g)$. It is obvious that the efficacy of the $O_2(^1\Delta_g)$ production is strongly dependent on the type of CMP. The highest conversions were achieved with 3D-PdTPP_CMP and 3D-TPP_CMP. The materials 2D-TPP_CMP and 2D-PdTPP_CMP are in the middle, and the lowest $O_2(^1\Delta_g)$ productivity was observed with 3D-DPP_CMP. These measurements approved the previous results (see above) that the 3D topology of CMPs is the most suitable for $O_2(^1\Delta_g)$ photosensitisation due to the smaller degree of stacking of the porphyrin units. The DPP building blocks are the only exception due to the short distance between the porphyrin units in the resulting structure. The repeated usage of CMPs as photosensitizers was also investigated. When 3D-PdTPP_CMP was used in the second run, the conversion of 9,10-diphenylanthracene reached 98 % after 3 h, in comparison with 96 % achieved in the first run. These results show that the CMPs retain their photosensitization activity and can be used repeatedly.

The photosensitization efficacy of porphyrin-based CMPs was compared with porphyrin MOFs. These MOFs have highly ordered crystalline structures and high pore volumes, and

therefore, high $O_2(^1\Delta_g)$ productivity was expected. Only water stable structures were selected from a wide range of existing porphyrin MOFs, namely, MOF-525,[33] PCN-222,[34] (Figure 9) and Al-TPPC MOF[91] (Figure 33) . The results show that PCN-222 and MOF-525 have comparable photosensitization activities to the least efficient 3D-DPP_CMP. Al-TPPC MOF is more than twice more efficient than PCN-222 and MOF-525, but the conversion is still below the vast majority of CMPs.

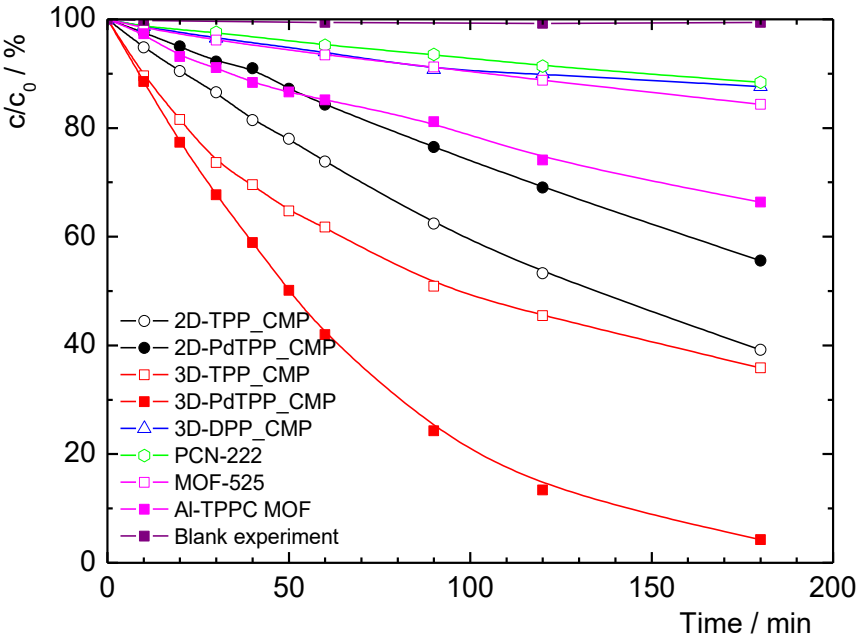

Figure 32. Reaction of photosensitized $O_2(^1\Delta_g)$ produced by CMP and MOF dispersions in acetonitrile with 9,10-diphenyl anthracene.

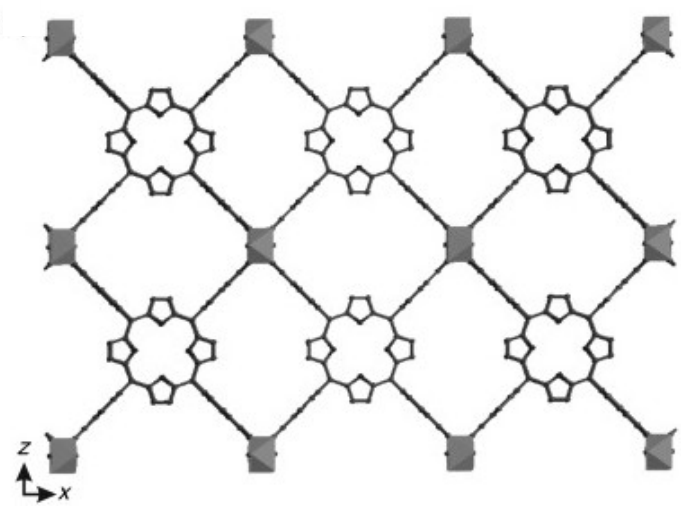

Figure 33. Structure of the Al-TPPC MOF.[91]

The $O_2(^1\Delta_g)$ productivity of porphyrin-based COFs is comparable to (3D-PdTPP_COF) or it is even higher than that of the structurally similar CMPs (2D-TPP_COF and 3D-TPP_COF) (see Figure 34).

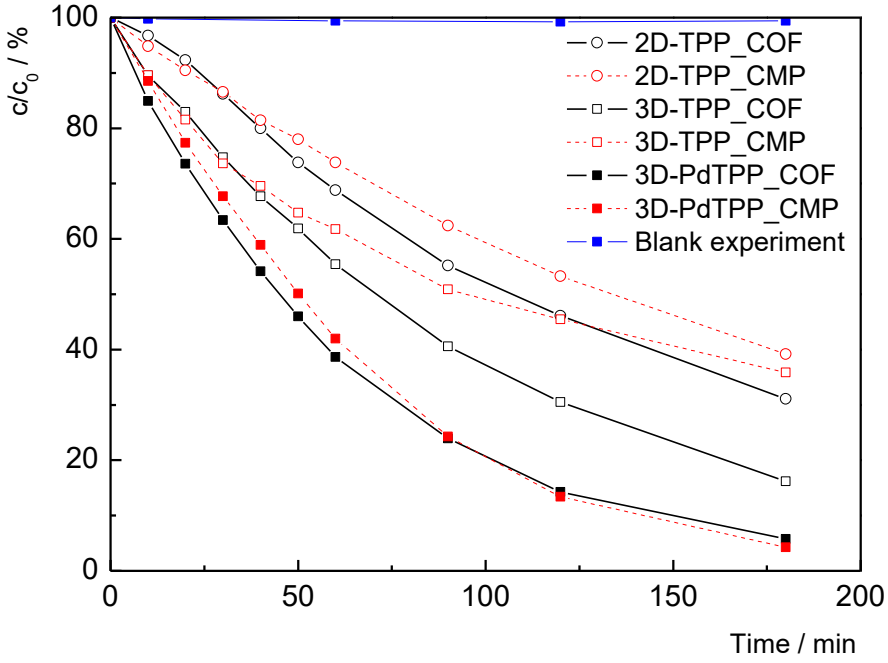

Figure 34. Reaction of photosensitized $O_2(^1\Delta_g)$ produced by COF dispersions in acetonitrile with 9,10-diphenylanthracene compared with structurally relevant CMPs. Blank experiment performed in the absence of COFs excluded any photoreaction of 9,10-diphenylanthracene itself.

3.1.5 Photobiological properties

Porphyrin-based CMPs proved to be very stable materials and potent $O_2(^1\Delta_g)$ producers, however, the absence of any polar groups at the polymer backbone complicates their potential use for biological applications. From this point of view, porphyrin-based COFs are supposed to be better. The presence of residual –CHO and $–NH_2$ groups increases the surface wettability and, additionally, $–NH_2$ groups are reported to provide stronger adhesion to bacterial cell walls.[92] For this reason, the investigated porphyrin-based COFs were employed for fabrication of antimicrobial coatings. The materials were dispersed in a polystyrene/(aminomethyl)polystyrene solution and the dispersions were drop-casted onto glass wafers.

The antimicrobial activity of the COF coatings was tested in collaboration with the Department of Biochemistry and Microbiology, University of Chemistry and Technology,

Prague (Dr. J. Zelenka, Prof. T. Ruml). The tests were performed with two potential pathogens, *Pseudomonas aeruginosa* and *Enterococcus faecalis*. At room temperature, both investigated bacteria strains form single-cell-thick biofilms after 24 h and multi-cell-thick films after 48 h. The COF coatings enabled the growth of bacteria biofilms in both cases, although their density was lower than the density on a bare polystyrene/(aminomethyl)polystyrene surface. Upon irradiation with 460 nm light, the formation of bacteria biofilms completely diminished on the COF coatings. When 525 nm light was employed, the 3D-TPP_COF coating efficiently suppressed the growth of *P. aeruginosa* biofilms, whereas 2D-TPP_COF and 3D-PdTPP_COF did not have any effect (Figure 35A). In the case of *E. faecalis* biofilms, all studied COF coatings had considerable antimicrobial activities using both 460 and 525 nm irradiation (Figure 35B).

Similar results were obtained with the coatings incubated for 48 h under irradiation with 460 nm light (Figure 35C). The growth of *E. faecalis* biofilms was inhibited by all COF coatings. Whereas the growth of *P. aeruginosa* biofilms was completely inhibited by 3D-TPP_COF, it was only partially mitigated by 2D-TPP_COF and 3D-PdTPP_COF coatings. According to the results of the experiments where the biofilms were first incubated for 24 h without irradiation followed by irradiation for another 4 h (see Figure 35D), the COF coatings can destroy even already formed *P. aeruginosa* and *E. faecalis* biofilms.

Summing up, the porphyrin COFs are potent antimicrobial agents, especially 3D-TPP_COF. They efficiently inhibit the growth of *P. aeruginosa* and *E. faecalis* biofilms under irradiation with 460 nm. The COFs also reveal antimicrobial activity under 525 nm light, however, the effect is less pronounced. This fact is probably a consequence of less effective light absorption in this spectral region. The COFs are stable during antimicrobial tests as the release of porphyrin from the frameworks was not observed.

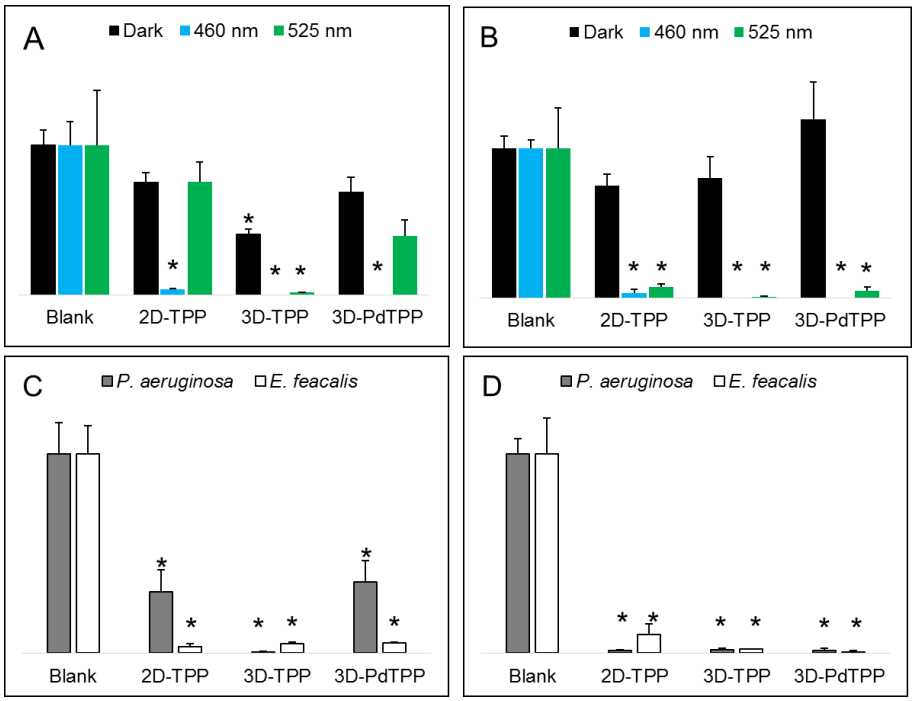

Figure 35. Antimicrobial activity of the COF coatings. The surfaces were incubated 24 h in the dark (black), and under 460 (20 mW cm^{-2}, blue) or 525 nm irradiation (7 mW cm^{-2}, green) with *P. aeruginosa* (A) and *E. faecalis* (B). Similar experiment was performed after 48 h incubation under 460 nm light (C). To test the direct killing of cells in the biofilms, the biofilms of *P. aeruginosa* and *E. faecalis* were established by 24 h incubation in the dark, followed by 4 h irradiation with 460 nm light (D).

3.2 Porphyrin phosphinic acids

Appendix III describes the synthesis of porphyrin derivatives with –PR(O)OH functional groups, their photophysical properties, and potential use for PDT of tumours.[93] These molecules were prepared with a perspective of use either as building blocks for MOFs or for postsynthetic modification of MOFs.

3.2.1 Synthesis and basic characterisation

The porphyrin phosphinic acids were synthesized in a three-step synthetic route depicted in Scheme 6. First step involved the preparation of monoalkyl/arylphosphinate precursors (**1a-c**) from commercially available monoalkyl/arylphosphine dichlorides. These compounds were used as reagents in Pd(0) catalysed P–C coupling reactions with 5,10,15,20-tetrakis(4-bromophenyl)porphyrine (TPPBr). Finally, obtained methyl porphyrinphosphinates (**2a-c**) underwent trimethylsilyl bromide-assisted deprotection, providing phosphinic acids **3a-c**.

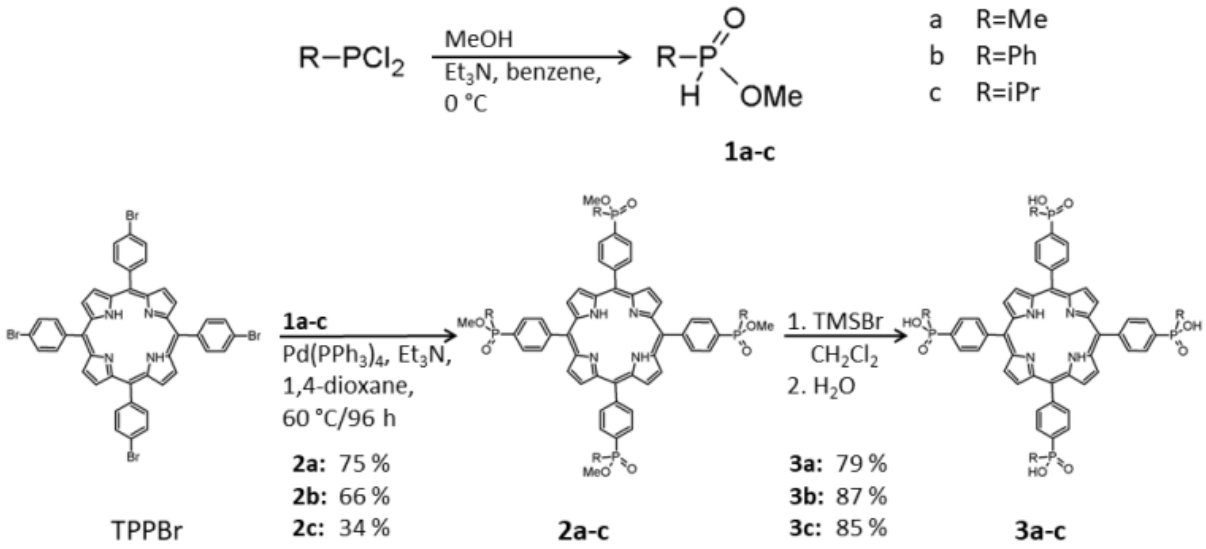

Scheme 6. Synthetic route to preparation of porphyrin phosphinic acids.

Compounds **2a-c** were characterized by ^{1}H, ^{31}P, and ^{13}C NMR spectroscopy and high-resolution mass spectrometry (HRMS). Due to their limited solubility in common organic solvents, compounds **3a-c** were characterized by HRMS only. The results of the characterization methods confirmed the expected composition of the prepared compounds.

To quantify the hydrophobicity of prepared porphyrin derivatives, 1-octanol/phosphate buffer saline (PBS) partition coefficients were determined (Table 4). The results display increasing hydrophobicity in the order **3a** << **3c** < **3b**. TPPS, which was used for comparison in all performed photophysical and biological studies, has the least hydrophobic nature among all investigated compounds, although the exact value of partition coefficient cannot be given because its concentration in the 1-octanol phase was below the detection limit of UV-vis.

3.2.2 Photophysical properties

Porphyrins **3a-c** display characteristic fluorescence bands at approximately 650 and 710 nm. Other measured characteristics are summarized in Table 4. The values of fluorescence quantum yields (Φ_f), fluorescence lifetimes (τ_f), triplet state lifetimes (τ_{T0}), quantum yields of singlet oxygen formation (Φ_Δ) as well as the calculated values of bimolecular rate constants of triplet state quenching by oxygen (k_{O2}) and the fraction of triplet states quenched by oxygen (F_T^{air}) well correspond to the characteristics of TPPS. These results indicate that peripheral substitution by phosphinic groups does not influence the overall photophysical properties of the compounds.

Table 4. Photophysical properties of the porphyrins in PBS.[a]

Porphyrin	logP_{OB}	Φ_f	τ_f/ns	τ_{T0}/μs	k_{O2}/$M^{-1}s^{-1}$	F_T^{air}	Φ_Δ
3a	–2.93	0.09	9.5	270	1.7×10^9	0.99	0.60
3b	–1.47	0.09	9.2	210	1.7×10^9	0.99	0.56
3c	–1.68	0.10	9.3	270	1.7×10^9	0.99	0.60
TPPS	–	0.08[b]	10.4[b]	330	1.7×10^9	1.00	0.62[c]

[a] logP_{OB} is the 1-octanol/PBS partition coefficient in the logarithmic scale, porphyrin concentrations were determined by UV-vis, Φ_f is the fluorescence quantum yield, excitation wavelengths were 414 and 517 nm; τ_f is the fluorescence lifetime, excitation wavelength was 405 nm; τ_{T0} stands for the lifetime of the porphyrin triplet states in argon-saturated PBS; k_{O2} is the bimolecular rate constant of the triplet state quenching by oxygen; $F_T^{air} = 1\text{-}\tau_T/\tau_{T0}$ is the fraction of the triplet states quenched by oxygen in air-saturated PBS; Φ_Δ is the quantum yield of singlet oxygen formation in D_2O, excited at 420 nm. [b] Literature value, ref [94] [c] Literature value, ref [95].

An important process which negatively affects photophysical properties of porphyrins is aggregation. Moreover, it has also negative impact on porphyrin bioavailability and accumulation in target cells. The formation of porphyrin aggregates is dependent on pH and due to the characteristic shift and broadening of absorption bands it can be monitored by UV-vis. Figure 36 demonstrates behaviour of the porphyrin phosphinic acids and TPPS in basic (pH ~ 12), mildly acidic (pH ~ 4), and strongly acidic (pH ~ 1) environment. In strongly acidic pH, compound **3a** and TPPS display protonation on pyrrole N atoms and partially also formation of well-ordered J-aggregates, which is documented by the occurrence of characteristic bands at approximately 434 and 490 nm, respectively. Under the same conditions, porphyrin **3b** forms non-specific aggregates with a broad band in the absorption spectrum at approximately 450 nm. At higher pH, aggregates of both **3a** and **3b** completely disappear. Compound **3c** does not reveal any aggregation even at pH ~1, and the absorption spectrum corresponds to a monomeric protonated form of porphyrin. This result points out that bulky substituents on P atoms, such as phenyl or isopropyl, efficiently protect porphyrin molecules against aggregation.

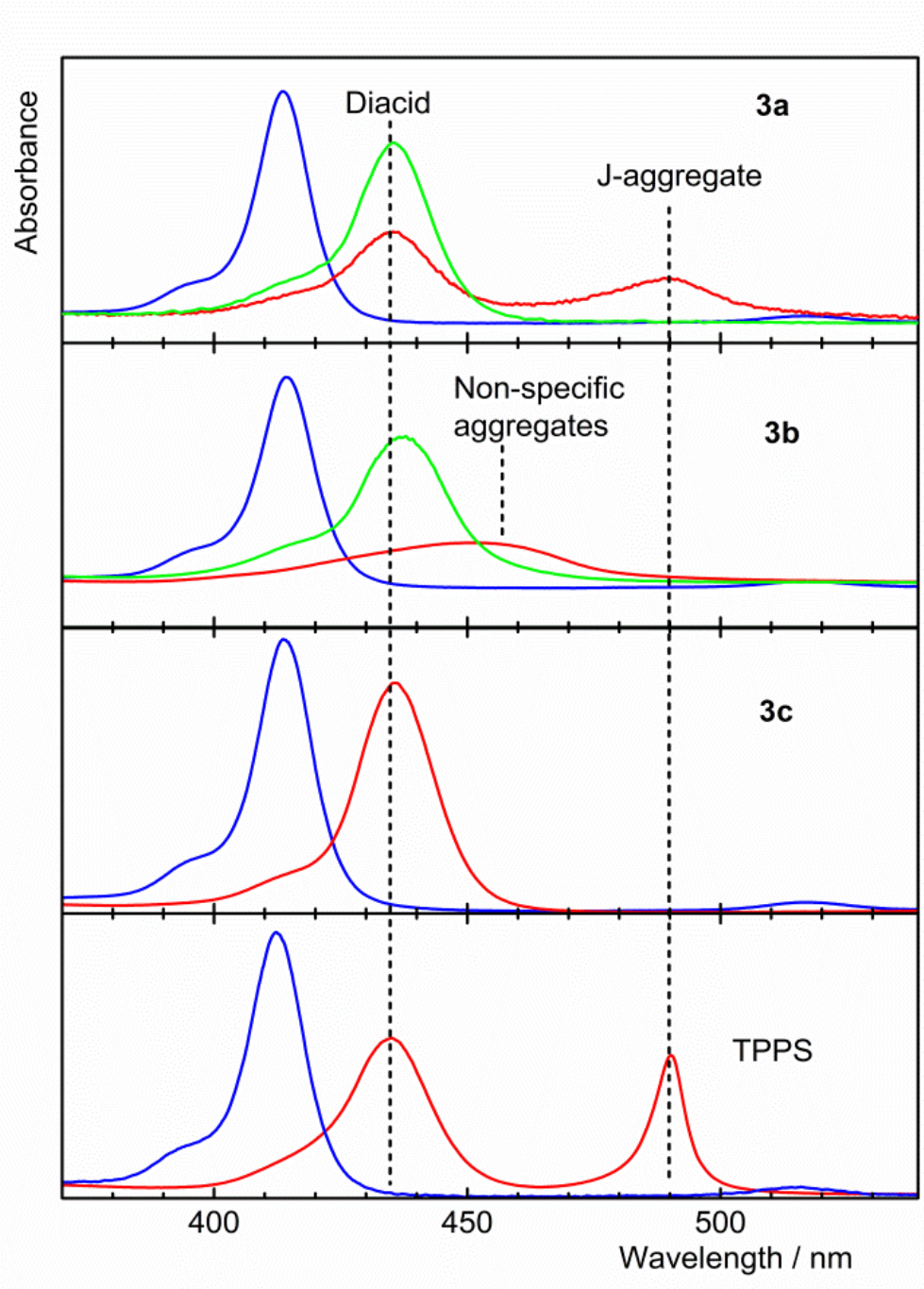

Figure 36. Absorption spectra of **3a**, **3b**, **3c**, and TPPS in the Soret region at pH ~1 (red), pH ~ 4 (green), and pH ~ 12 (blue) indicating differences in aggregation properties.

Albumin is a ubiquitous protein in human body which significantly influences transport and cellular accumulation of drugs. For this reason, binding of the studied porphyrins to human serum albumin (HSA) was investigated. The strength of binding is quantified by binding constants (K_b) calculated by nonlinear fitting analysis of binding isotherms depicted in Figure 37. The K_b values for compounds **3a-c** and TPPS are 9.8×10^4, 1.5×10^6, 7.7×10^5 and 2.5×10^6 M^{-1}, respectively. The affinity of porphyrins towards HSA increases in the order

3a << **3c** < **3b** < TPPS. The significant differences in the values of K_b for particular porphyrins point out that the substituent on P atoms plays an important role in the behaviour of the compounds in biological systems.

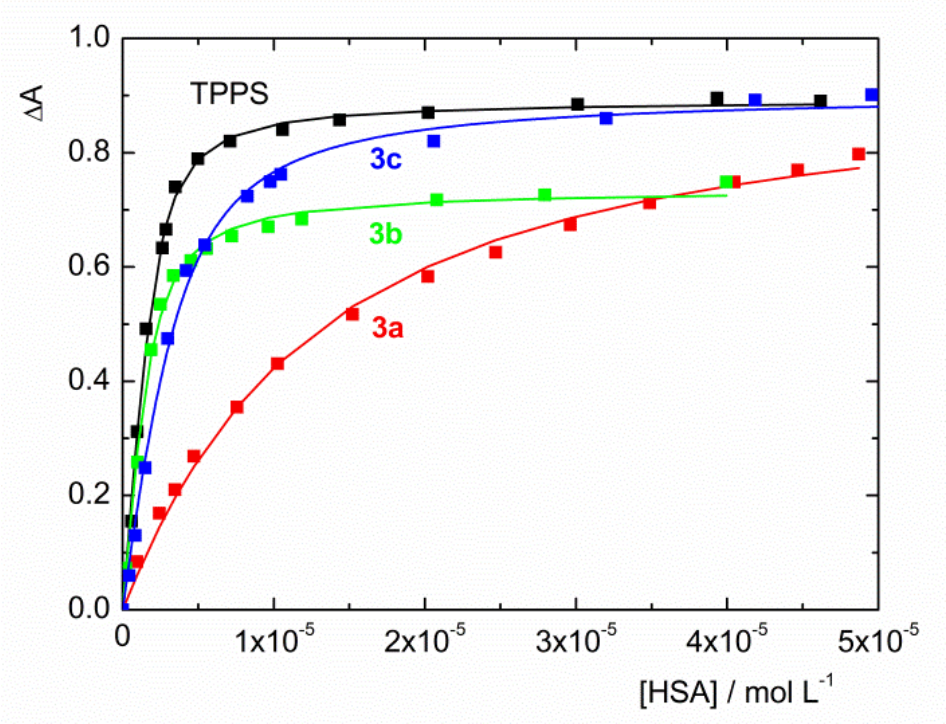

Figure 37. Binding isotherms of TPPS and **3a** - **3c** with HSA in PBS. Full lines represent corresponding non-linear fits.

3.2.3 Application for PDT

The cytotoxic activity of the compounds was tested by collaborators at the Department of Biochemistry and Microbiology, University of Chemistry and Technology, Prague (Dr. J. Zelenka, Prof. T. Ruml). The tests were realised on two cell lines: cancerous HeLa cells and non-cancerous MRC-5. According to the results of the tests performed without irradiation (Figure 38A and B), the compounds themselves are toxic neither for cancerous nor for non-cancerous cells up to the concentration of 10 μM. The relative cell viability after 15 min irradiation with a halogen lamp (Figure 38C and D) reveals significant differences among particular porphyrins. Interestingly, porphyrin **3a** does not display any photocytotoxic effect, whereas other prepared derivatives **3b** and **3c** kill cancerous cells even more effectively than commercially available porphyrins TPPC and TPPS used as standards for comparison. Especially porphyrin **3c** demonstrates superior photocytotoxic effect, even for non-cancerous MRC-5 cells. The overall photocytotoxic efficiency of the investigated porphyrins increases in the order **3a** < TPPS ~ TPPC < **3b** < **3c**. Similar behaviour was observed also when 525 nm

light was applied (Figure 38E and F). The half maximal effective concentration (EC_{50}) values of **3c** are 0.63 and 0.45 μM for irradiation with a halogen lamp and 525 nm light, respectively.

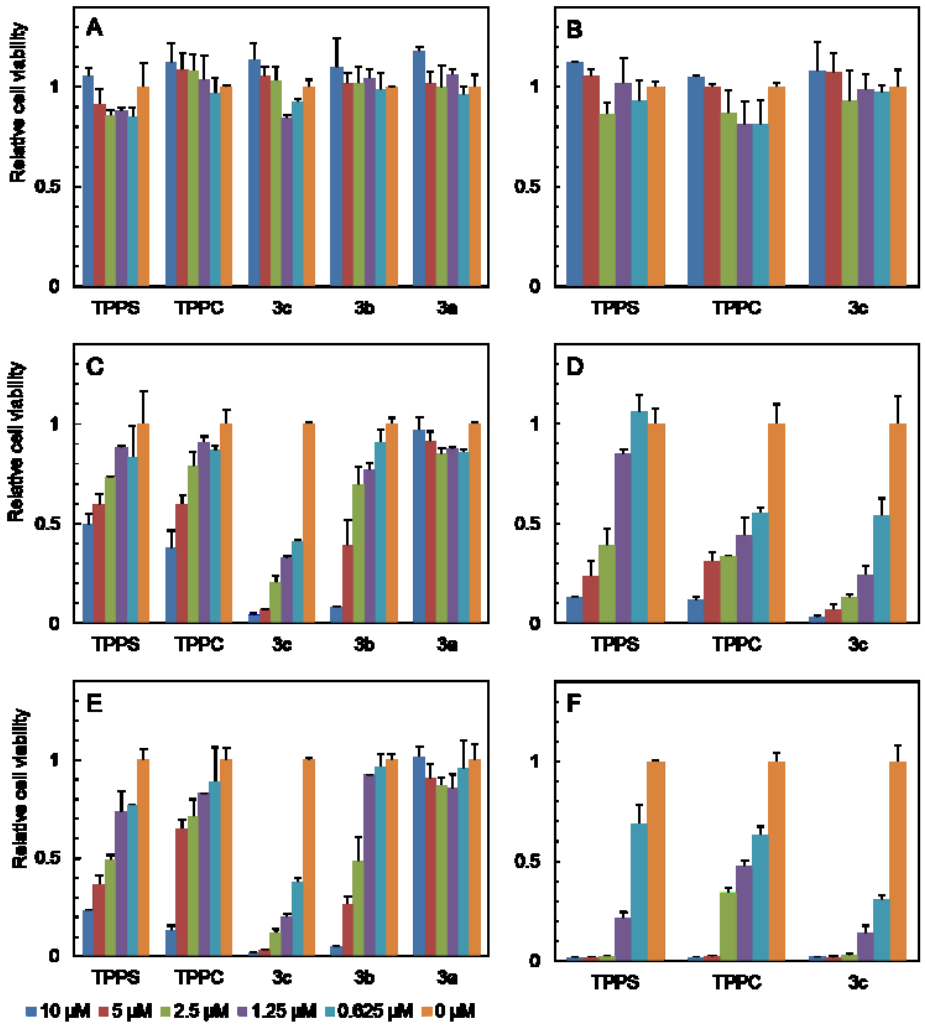

Figure 38. Relative viability of HeLa (A, C, E) and MRC-5 (B, D, F) cells incubated with porphyrins: (A, B) Dark toxicity – 24 h incubation in dark; (C, D) Photocytotoxicity – 24 h incubation followed by 15 min irradiation with a 150 W halogen lamp, 45 mW cm^{-2}; (E, F) Photocytotoxicity - 24 h incubation followed by 15 min irradiation with 525 nm light, 9 mW cm^{-2}. Note: The results labelled 0 μM indicate the control experiments with the cells not incubated with porphyrins.

To investigate the origin of different photocytotoxicity, the cellular uptake was determined by measuring porphyrin fluorescence intensity of HeLa cells after their incubation in the porphyrin-containing medium. Figure 39A shows that the compound with the highest photocytotoxicity (**3c**) has also the highest cellular uptake. On the other hand, the least efficient porphyrin **3a** is internalized by the cells with the lowest efficiency. The extent of the

cellular uptake increases with porphyrin concentration in the medium and incubation time (Figure 39B and C).

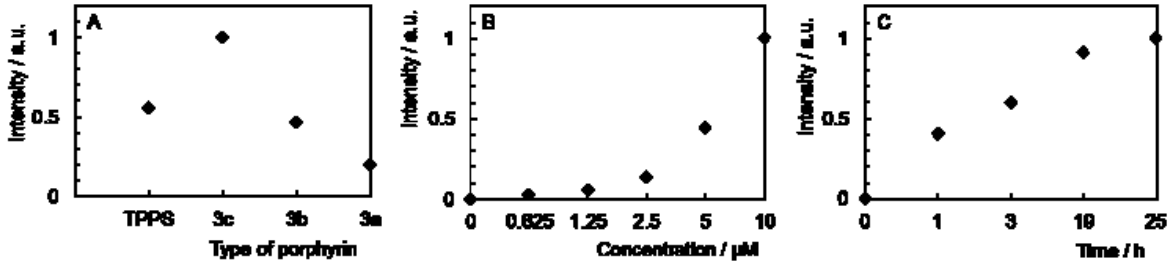

Figure 39. Porphyrin uptake by HeLa cells determined by flow cytometry: (A) Uptake of porphyrins relatively to porphyrin **3c** (24 h incubation with 1.25 μM porphyrin); (B) Concentration-dependent uptake of **3c**, 24 h incubation; (C) Time-dependent uptake of 0.625 μM **3c**, 24 h incubation. The axis *y* represents the relative fluorescence intensity of the cells.

An important parameter which influences photocytotoxicity of compounds is their intracellular localisation. Results from spinning disc confocal microscopy show that porphyrin **3c** is co-localised with lysosomes as visualized by LysoTracker Green dye (Figure 40). Lysosomes are important cell organelles responsible for cell homeostasis and specific delivery of therapeutics to lysosomes is beneficial for their effectivity. Interestingly, porphyrin **3c** is co-localised with lysosomes similarly to much more hydrophilic TPPS. Co-localisation of **3c** with lysosomes can be one of the reasons for strong photocytotoxic effect of this compound.

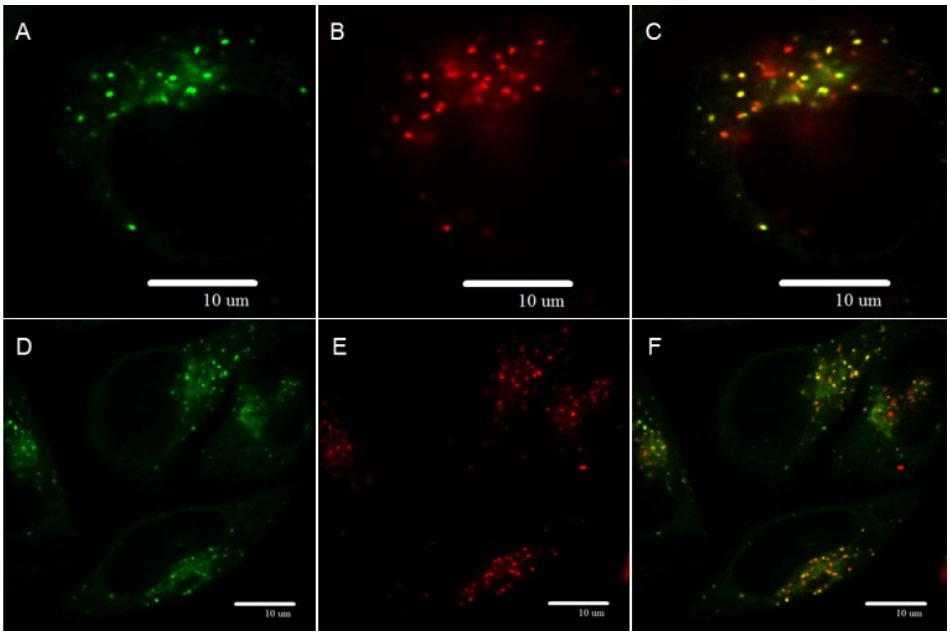

Figure 40. Confocal microscopy of HeLa cells incubated with 1.25 μM **3c** for 24 hours: (A, D) LysoTracker Green; (B, E) porphyrin **3c**; (C, F) overlay. White bars correspond to 10 μm.

Another reason for different photocytotoxicity of the studied porphyrins might be connected with variations of their retention in cells. To characterize this effect, an experiment comparing TPPS, TPPC, and **3c** was performed. HeLa cells were first incubated with porphyrins and then the medium was exchanged for a fresh medium without porphyrin. Cells were irradiated 6 or 24 h after immersion in the porphyrin-free medium (Figure 41). In the case of **3c**, the photocytotoxic effect did not change after 6 h of immersion in the fresh medium, whereas the photocytotoxicity of both TPPC and TPPS completely disappeared. After 24 h wash-out, the photocytotoxicity of **3c** decreased; however, it was still much higher than the photocytotoxicity of the other studied porphyrins (compare Figures 38 and 41). The EC_{50} values of **3c** after 6 and 24 h wash-out are 0.72 and 2.31 μM, respectively. The results of the experiment demonstrate that compound **3c** has much stronger retention in HeLa cells than TPPC or TPPS.

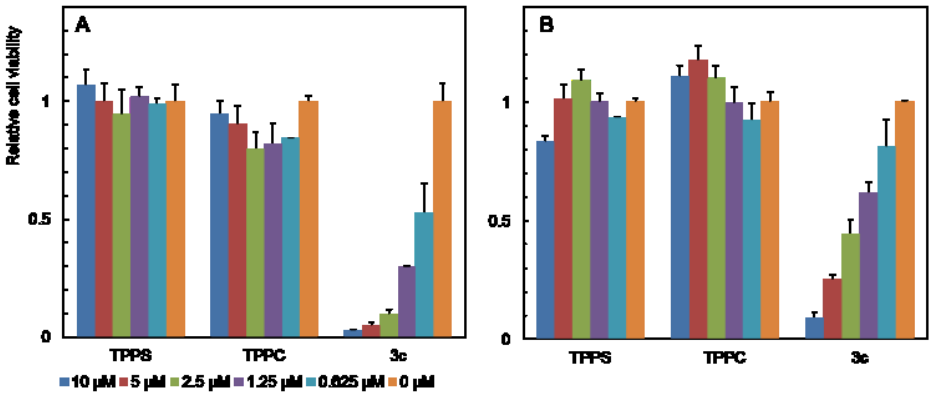

Figure 41. Relative viability of HeLa cells incubated with porphyrins for 24 h followed by washing with the medium and immersion in the fresh medium without porphyrins for 6 (A) and 24 h (B); 15 min irradiation with a halogen lamp, 45 mW cm^{-2}. Note: The results labelled 0 μM indicate the control experiments with the cells not incubated with porphyrins.

The investigation of the photodynamic efficacy of the porphyrin phosphinic acids showed significant differences. According to the performed studies, it is a consequence of multiple factors including the tendency towards aggregation, strength of the binding to serum albumin, and different hydrophobicity of the compounds affecting their cellular uptake and retention in cells. Evidently, different photoactivities are not caused by changes in photophysical properties of the porphyrins which were found to be the same in all cases, regardless of the peripheral substitution.

3.2.4 Coordination polymers based on porphyrin phosphinates

Porphyrins **3a-c** were used for the synthesis of coordination polymers structurally similar to ICR-2 (structure shown in Figure 8). A range of coordination polymers was prepared by a solvothermal method, starting from different porphyrins (**3a-c**) and metals (Fe(III), Zr(IV)), varying the solvents (water, *N,N*-dimethylformamide, ethanol) and temperatures (100 – 250 °C). The resulting solids did not show satisfactory XRD patterns, evidencing their disordered nature. The material with the highest crystallinity was prepared from porphyrin **3b** and $FeCl_3$ in water with an addition of hydrofluoric acid at 250 °C for 96 h. However, the crystallinity of this material was too low to allow structural determination (Figure 42). In addition, the adsorption of N_2 did not confirm desired porous character of this coordination polymer. These properties are not suitable for the proposed application of these MOFs as photosensitizers of $O_2(^1\Delta_g)$, and therefore all other attempts to synthesize these MOFs were abandoned.

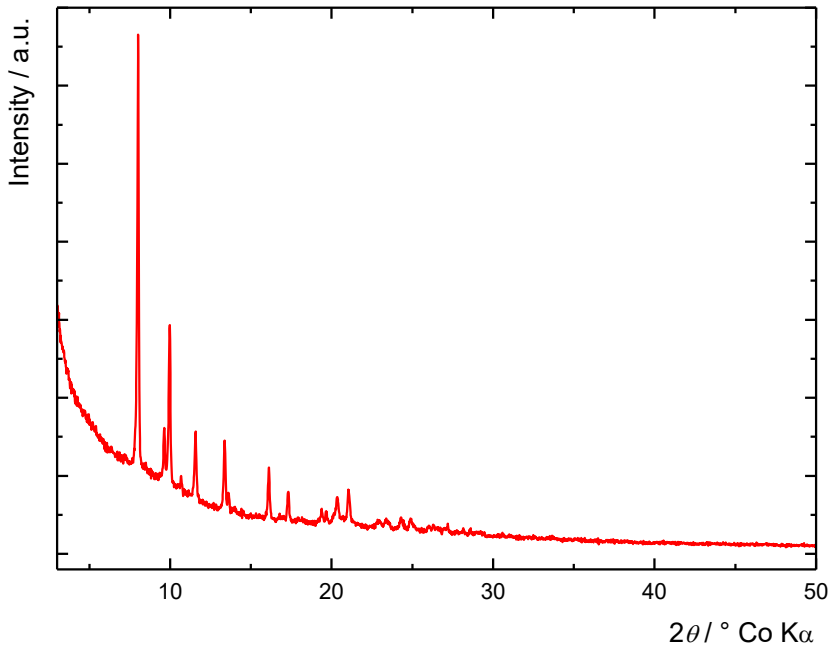

Figure 42. XRD pattern of a coordination polymer synthesized from **3b** and Fe(III) in the presence of HF at 250 °C for 96 h.

Although all attempts to crystallize porous frameworks using porphyrins **3a-c** as linkers were unsuccessful, porphyrins **3a-c** were utilized for the modification of the nanoparticles derived from ICR-2. The nanoICR-2/porphyrin composites retain the photophysical properties of free porphyrins and the photodynamic efficacy of thus modified nanoparticles is strongly affected by substitution on P atoms.[96]

4 Conclusions

New photoactive porphyrin-containing porous polymers were synthesized, their structure and composition was characterised by N_2 adsorption, XRD, FTIR and solid-state NMR spectroscopy, and their photophysical properties were characterized by UV-vis, fluorescence and transient spectroscopy. Since the porous polymers proved to be efficient solid photosensitizers of $O_2(^1\Delta_g)$, they were utilized in the area of photodynamic inactivation of bacteria. Also, new porphyrin phosphinic acids were synthesized, and it was demonstrated that these porphyrins are attractive candidates for photodynamic applications since their photodynamic efficacy can be tuned by substitution on phosphorus atoms.

The results can be summarized in following points:

1. Porphyrin-containing CMPs are efficient solid photosensitizers of $O_2(^1\Delta_g)$, much more efficient than porphyrin-based MOFs in spite of their one order of magnitude lower specific surface area.
2. The CMPs productivity of $O_2(^1\Delta_g)$ is strongly dependent on their structure. The frameworks with the 3D topology are more efficient than those with the 2D topology. The size of building blocks plays an important role; too low distance between neighbouring porphyrin units significantly suppresses the yields of $O_2(^1\Delta_g)$.
3. Incorporation of porphyrins into the structure of COFs effectively eliminates aggregation of porphyrin moieties. The photophysical characteristics of resulting materials (fluorescence and phosphorescence lifetimes, quantum yield of $O_2(^1\Delta_g)$ formation, etc.) are very close to those values of molecular porphyrins in solutions.
4. Porphyrin-containing COFs are hydrolytically stable and can be used for the inhibition of the bacteria biofilm growth.
5. Substitution of tetraphenylporphyrin with phosphinic groups does not affect the photophysical characteristics of the molecules. Varying the substituent on phosphorus atoms enables tuning the hydrophilic/hydrophobic character of the molecules, which has a strong influence on their behaviour in biological systems.
6. Tetraphenylporphyrin substituted with isopropylphosphinic groups has the highest photodynamic efficacy from all investigated porphyrins. Its favourable properties are a consequence of moderate binding to serum albumin, low tendency towards aggregation, high cellular uptake, and high retention in the cells.

7. Porphyrin phosphinic acids can be successfully used for a postsynthetic modification of MOF nanoparticles.

4.1 Author's contributions

Since the work involved synthesis of the materials, adsorption, and photophysical measurements and biological experiments, it was realised in the team of synthetic and physical chemists, and biologists. To the results presented in the thesis, the author contributed by the following items:

- Design and the syntheses of all CMPs and COFs including the syntheses of their precursors.
- Characterisation of all precursors and materials by NMR, FTIR, and UV-vis spectroscopy, analysis of emission spectra.
- Testing of the materials for production of $O_2(^1\Delta_g)$.
- Preparation of the antimicrobial COF coatings used for biological testing.
- Synthesis of porphyrin phosphinic acids and their characterisation by NMR.
- Writing of the papers, interpretation of the results, dealing with referee comments during the peer review process.

5 References

[1] M. Urbani, M. Grätzel, M. K. Nazeerudin, T. Torres, *Chem. Rev.* **2014**, *114*, 12330–12396.

[2] A. Blázques-Castro, *Redox Biol.* **2017**, *13*, 39–59.

[3] Z. Juračková, in *Volné radikály a antioxidanty v medicíně (I)*, p. 55-71, Ed. Z. Juračková, Slovak Academic Press, Bratislava, **1998**.

[4] M. Johnsen, M. J. Paterson, J. Arnbjerg, O. Christiansen, C. B. Nielsen, M. Jørgensen, P. R. Ogilby, *Phys. Chem. Chem. Phys*. **2008**, *10*, 1177–1191.

[5] C. S. Foote, *Photochem. Photobiol.* **1991**, *54*, 659–659.

[6] K. Lang, J. Mosinger, D. M. Wagnerová, *Coor. Chem. Rev.* **2004**, *248*, 321–350.

[7] K. Lang, P. Bezdička, J. L. Bourdelande, J. Hernando, I. Jirka, E. Káfuňková, F. Kovanda, P. Kubát, J. Mosinger, D. M. Wagnerová, *Chem. Mater.* **2006**, *19*, 3822–3829.

[8] J. Demel, P. Kubát, I. Jirka, P. Kovář, M. Pospíšil, K. Lang, *J. Phys. Chem. C* **2010**, *114*, 16321–16328.

[9] M. Jiřičková, J. Demel, P. Kubát, J. Hostomský, F. Kovanda, K. Lang, *J. Phys. Chem. C* **2011**, *115*, 21700–21706.

[10] J. Demel, P. Kubát, F. Millange, J. Marrot, I. Císařová, K. Lang, *Inorg. Chem.* **2013**, *52*, 2779–2786.

[11] M. C. DeRosa, R. J. Crutchley, *Coor. Chem. Rev.* **2002**, *352*, 233–234.

[12] F. Böhm, R. Edge, S. Foley, L. Lange, T. G. Truscott, *J. Photochem. Photobiol. B: Biol.* **2001**, *65*, 177–183.

[13] J. Kou, D. Dou, L. Yang, *Onkotarget* **2017**, *8*, 81591–81603.

[14] M. R. Hamblin, *Curr. Opin. Microbiol.* **2016**, *33*, 67–73.

[15] J. T. Ferreira, J. Pina, C. A. F. Ribeiro, R. Fernandes, J. P. C. Tomé, M. S. Rodríguez-Morgade, T. Torres, *J. Mater. Chem. B* **2017**, *5*, 5862–5869.

[16] Z. Huang, *Technol. Cancer Res. Treat.* **2005**, *4*, 283–293.

[17] J. Zhang, C. Jiang, J. P. F. Longo, R. B. Azevedo, H. Zhang, L. A. Muehlmann, *Acta Pharmacol. Sin. B* **2018**, *8*, 137–146.

[18] L. B. Josefsen, R. W. Boyle, *Br. J. Pharmacol.* **2008**, *154*, 1–3.

[19] R. Weijer, M. Broekgaarden, R. F. van Golen, E. Bulle, E. Nieuwenhuis, A. Jongejan, P. D. Moerland, A. H. C. van Kampen, T. M. van Gulik, M. Heger, *BMC Cancer* **2015**, *14*, 1014–1030.

[20] M. R. Hamblin, *Curr. Opin. Microbiol.* **2016**, *33*, 67–73.

[21] C. F. Pereira, M. M. Q. Simoes, J. P. C. Tomé, F. A. Almeida Paz, *Molecules* **2016**, *21*, 1348–1366.

[22] O. M. Yaghi, H. Li, *J. Am. Chem. Soc.* **1995**, *117*, 10401–10402.

[23] H. Li, M. Eddaoudi, M. O'Keeffe, O. M. Yaghi, *Nature* **1999**, *402*, 276–279.

[24] M. Eddaoudi, J. Kim, N. Rosi, D. Vodak, J. Wachter, M. O'Keeffe, O. M. Yaghi, *Science* **2002**, *295*, 469–472.

[25] C. Serre, F. Millange, C. Thouvenot, M. Nogues, G. Marsolier, D. Louër, G. Férey, *J. Am. Chem. Soc.* **2002**, *124*, 13519–13526.

[26] I. Berverkhyy, G. Ortiz, G. Chaplais, C. Marichal, G. Weber, J.-P. Bellat, *Microporous Mesoporous Mater.* **2014**, *183*, 156–161.

27 G. Férey, C. Mellot-Draznieks, C. Serre, F. Millange, J. Dutour, S. Surblé, I. Margiolaki, *Science* **2005**, *309*, 2040–2042.

[28] J. H. Cavka, S. Jakobsen, U. Olsbye, N. Guillou, C. Lamberti, S. Bordiga, K. P. Lillerud, *J. Am. Chem. Soc.* **2008**, *130*, 13850–13851.

[29] Y. Bai, Y. Dou, L.-H. Xie, W. Rutledge, J.-R. Li, H.-C. Zhou, *Chem. Soc. Rev.* **2016**, *45*, 2327–2367.

[30] J. Hynek, P. Brázda, J. Rohlíček, M. G. S. Londesborough, J. Demel, *Angew. Chem. Int. Ed.* **2018**, *57*, 5016–5019.

[31] P. M. Barron, C. A. Wray, C. Hu, Z. Guo, W. Choe, *Inorg. Chem.* **2010**, *49*, 10217–10219.

[32] S. Huh, S.-J. Kim, Y. Kim, *CrystEngComm* **2016**, *18*, 345–368.

[33] W. Morris, B. Volosskiy, S. Demir, F. Gándara, P. L. McGrier, H. Furukawa, D. Cascio, J. F. Stoddart, O. M. Yaghi, *Inorg. Chem.* **2012**, *51*, 6443–6445.

[34] D. Feng, Z.-Y. Gu, J.-R. Li, H.-L. Jiang, Z. Wei, H.-C. Zhou, *Angew. Chem. Int. Ed.* **2012**, *51*, 10307–10310.

[35] C. S. Diercks, O. M. Yaghi, *Science* **2017**, *355*, aal1585.

[36] F. Beuerle, B. Gole, *Angew Chem. Int. Ed.* **2018**, *57*, 4850–4878.

[37] A. P. Côté, A. I. Benin, N. W. Ockwig, M. O'Keeffe, A. J. Matzger, O. M. Yaghi, *Science* **2005**, *310*, 1166–1170.

[38] K. T. Jackson, T. E. Reich, H. M. El-Kaderi, *Chem. Commun.* **2012**, *48*, 8823–8825.

[39] J. R. Hunt, C. J. Doonan, J. D. LeVangie, A. P. Côté, O. M. Yaghi, *J. Am. Chem. Soc.* **2008**, *130*, 11872–11873.

[40] Y. Du, H. Yang, J. M. Whiteley, S. Wan, Y. Jin, S.-H. Lee, W. Zhang, *Angew Chem. Int. Ed.* **2016**, *55*, 1737–1741.

[41] J. L. Segura, M. J. Mancheño, F. Zamora, *Chem. Soc. Rev.* **2016**, *45*, 5635–5671.

[42] F. J. Uribe-Romo, J. R. Hunt, H. Furukawa, C. Klöck, M. O'Keeffe, O. M. Yaghi, *J. Am. Chem. Soc.* **2009**, *131*, 4570–4571.

[43] S. Dalapati, S. Jin, J. Gao, Y. Xu, A. Nagai, D. Jiang, *J. Am. Chem. Soc.* **2013**, *135*, 17310–17313.

[44] F. J. Uribe-Romo, C. J. Doonan, H. Furukawa, K. Oisaki, O. M. Yaghi, *J. Am. Chem. Soc.* **2011**, *133*, 11478–11481.

[45] R. W. Tilford, W. R. Gemmil, H.-C. Zur Loye, J. J. Lavigne, *Chem. Mater.* **2006**, *18*, 5296–5301.

[46] E. L. Spitler, W. R. Dichtel, *Nat. Chem.* **2010**, *2*, 672–677.

[47] X. Feng, L. Chen, Y. Dong, D. Jiang, *Chem. Commun.* **2011**, *47*, 1979 –1981.

[48] X. Ding, J. Guo, X. Feng, Y. Honsho, J. Guo, S. Seki, P. Maitarad, A. Saeki, S. Nagase, D. Jiang, *Angew. Chem. Int. Ed.* **2011**, *50*, 1289–1293.

[49] S. Wan, F. Gándara, A. Asano, H. Furukawa, A. Saeki, S. K. Dey, L. Liao, M. W. Ambrogio, Y. Y. Botros, X. Duan, S. Seki, J. F. Stoddart, O. M. Yaghi, *Chem. Mater.* **2011**, *23*, 4094–4097.

[50] S. Kandambeth, D. B. Shinde, M. K. Panda, B. Lukose, T. Heine, R. Banerjee, *Angew. Chem. Int. Ed.* **2013**, *52*, 13052–13056.

[51] X. Chen, M. Addicoat, E. Jin, L. Zhai, H. Xu, N. Huang, Z. Guo, L. Liu, S. Irle, D. Jiang, *J. Am. Chem. Soc.* **2015**, *137*, 3241–3247.

[52] A. Nagai, X. Chen, X. Feng, X. Ding, Z. Guo, D. Jiang, *Angew. Chem. Int. Ed.* **2013**, *52*, 3770–3774.

[53] Y. Hu, N. Goodeal, Y. Chen, A. M. Ganose, R. G. Palgrave, H. Bronstein, M. O. Blunt, *Chem. Commun.* **2016**, *52*, 9941–9944.

[54] C. Zhang, S. Zhang, Y. Yan, F. Xia, A. Huang, Y. Xian, *ACS Appl. Mater, Interfaces* **2017**, *9*, 13415–13421.

[55] B. J. Smith, N. Hwang, A. D. Chavez, J. L. Novotney, W. R. Dichtel, *Chem. Commun.* **2015**, *51*, 7532–7535.

[56] H. M. El-Kaderi, J. R. Hunt, J. L. Mendoza-Cortés, A. P. Côté, R. E. Taylor, M. O'Keeffe, O. M. Yaghi, *Science* **2007**, *316*, 268–272.

[57] H. Ma, H. Ren, S. Meng, Z. Yan, H. Zhao, F. Sun, G. Zhu, *Chem. Commun.* **2013**, *49*, 9773–9775.

[58] Q. Fang, J. Wang, S. Gu, R. B. Kaspar, Z. Zhuang, J. Zheng, H. Guo, S. Qiu, Y. Yan, *J. Am. Chem. Soc.* **2015**, *137*, 8352–8355.

[59] G. Lin, H. Ding, D. Yuan, B. Wang, C. Wang, *J. Am. Chem. Soc.* **2016**, *138*, 3302–3305.

[60] G. Lin, H. Ding, R. Chen, Z. Peng, B. Wang, C. Wang, *J. Am. Chem. Soc.* **2017**, *139*, 8705–8709.

[61] A. I. Cooper, *Adv. Mater.* **2009**, *21*, 1291–1295.

[62] G. Zhu, H. Ren, *Porous Organic Frameworks – Design, Synthesis and Their Advanced Applications*, Spinger-Verlag, Berlin Heidelberg, **2015**.

[63] N. B. McKeown, S. Makhseed, P. M. Budd, *Chem. Commun.* **2002**, *2*, 2780–2781.

[64] N. B. McKeown, S. Hanif, K. Msayib, C. E. Tattershall, P. M. Budd, *Chem. Commun.* **2002**, *2*, 2782–2783.

[65] J. X. Jiang, A. I. F. Su, A. Trewin, C. D. Wood, N. L. Campbell, H. Niu, C. Dickinson, A. Y. Ganin, M. J. Rosseinsky, Y. Z. Kimyak, A. I. Cooper, *Angew. Chem. Int. Ed.* **2007**, *46*, 8574–8578.

[66] T. Ben, H. Ren, M. Shengqian, D. Cao, J. Lan, X. Jing, W. Wang, J. Xu, F. Deng, J. M. Simmons, S. Qiu, G. Zhu, *Angew. Chem. Int. Ed.* **2009**, *48*, 9457–9460.

[67] N. B. McKeown, P. M. Budd, *Chem. Soc. Rev.* **2006**, *35*, 675–683.

[68] S. Xu, B. Tan, *Microporous Organic Polymers: Sythesis, Types and Applications*, John Wiley & Sons, New York City, **2014**.

[69] Z. Kang, L. Fan, D. Sun, *J. Mater. Chem. A* **2017**, *5*, 10073–10091.

[70] Y.-S. Kang, Y. Lu, K. Chen, Y. Zhao, P. Wang, W.-Y. Sun, *Coor. Chem. Rev.* DOI: 10.1016/j.ccr.2018.02.009.

[71] Y.-B. Zhou, Z.-P. Zhan, *Chem. Asian J.* **2018**, *13*, 9–19.

[72] B. Yuan, Y. Pan, Y. Li, B. Yin, H. Jiang, *Angew. Chem. Int. Ed.* **2010**, *49*, 4054–4058.

[73] P. Horcajada, C. Serre, M. Vallet-Regí, M. Sebban, F. Taulelle, G. Férey, *Angew. Chem. Int. Ed.* **2006**, *45*, 5974–5978.

[74] M.-X. Wu, Y.-W. Yang, *Adv. Mater.* **2017**, *29*, 1606134.

[75] W. J. Rieter, K. M. L. Taylor, H. An, W. Lin, W. Lin, *J. Am. Chem. Soc.* **2006**, *128*, 9024–9025.

[76] S.-L. Li, Q. Xu, *Energy Enciron, Sci.* **2013**, *6*, 1656–1683.

[77] Z.-D. Yang, W. Wu, X. C. Zeng, *J. Mater. Chem. C* **2014**, *2*, 2902–2907.

[78] D. Feng, W.-C. Chung, Z. Wei, Z.-Y. Gu, H.-L. Jiang, Y.-P. Chen, D. J. Darensbourg, H.-C. Zhou, *J. Am. Chem. Soc.* **2013**, *135*, 17105–17110.

[79] L. Chen, Y. Yang, D. Jiang, *J. Am. Chem. Soc.* **2010**, *132*, 9138–9143.

[80] J. C. Barona-Castaño C. C. Carmona-Vargas, T. J. Brocksom, K. T. de Oliveira, *Molecules* **2016**, *21*, 310–336.

[81] J. Yang, Z. Wang, K. Hu, Y. Li, J. Feng, J. Shi, J. Gu, *ACS Appl. Mater. Interfaces* **2015**, *7*, 11956–11964.

[82] Y. Liu, A. J. Howarth, J. T. Hupp, O. K. Farha, *Angew. Chem. Int. Ed.* **2015**, *54*, 9001–9005.

[83] D. Bůžek, J. Zelenka, P. Ulbrich, T. Ruml, I. Křížová, J. Lang, P. Kubát, J. Demel, K. Kirakci, K. Lang, *J. Mater. Chem. B* **2017**, *5*, 1815–1821.

[84] W. Zhou, S. Begum, Z. Wang, P. Krolla, D. Wagner, S. Bräse, C. Wöll, M. Tsotsalas, *ACS Appl. Mater. Interfaces* **2018**, *10*, 1528–1533.

[85] M. Lismont, L. Dreesen, S. Wuttke, *Adv. Funct. Mater.* **2017**, *27*, 1606314.

[86] J. Hynek, S. Ondrušová, D. Bůžek, P. Kovář, J. Rathouský, J. Demel, *Chem. Commun.* **2017**, *53*, 8557–8560.

[87] J. Hynek, J. Rathouský, J. Demel, K. Lang, *RSC Adv.* **2018**, *6*, 44279–44287.

[88] J. Hynek, J. Zelenka, J. Rathouský, P. Kubát, T. Ruml. J. Demel, K. Lang, *ACS Appl. Mater. Interfaces* **2018**, *10*, 8527–8535.

[89] M. Bregnhoj, M. Westberg, F. Jensen, P. R. Ogilby, *Phys. Chem. Chem. Phys.* **2016**, *18*, 22946–22961.

[90] R. Schmidt, E. Afshari, *J. Phys. Chem.* **1990**, *94*, 4377–4378.

[91] A. Fateeva, P. A. Chater, C. P. Ireland, A. A. Tahir, Y. Z. Khimyak, P. V. Wiper, J. R. Darwent, M. J. Rosseinsky, *Angew. Chem. Int. Ed.* **2012**, *51*, 7440–7444.

[92] L. Mamone, D. D. Ferreyra, L. Gándara, G. Di Venosa, P. Vallecorsa, D. Sáenz, G. Calvo, A. Batlle, F. Buzzola, E. N. Durantini, A. Casas, *J. Photochem. Photobiol. B* **2016,** *161*, 222–229.

[93] J. Hynek, M. Koncošová, J. Zelenka, I. Křížová, T. Ruml, P. Kubát, J. Demel, K. Lang, *Org. Biomol. Chem.* **2018**, *16*, 7274–7281.

[94] K. Kalyanasundaram, M. Neumann-Spallart, *J. Phys. Chem.* **1982**, *86*, 5163–5169.

[95] F. Wilkinson, W. P. Helman, A. B. Ross, *J. Phys. Chem. Ref. Data*, **1993**, *22*, 113–262.

[96] J. Hynek, S. Jurík, M. Koncošová, J. Zelenka, I. Křížová, T. Ruml, K. Kirakci, I. Jakubec, F. Kovanda, K. Lang, J. Demel, *Beilstein J. Nanotechnol.* **2018**, *9*, 2960–2967.